CO2 ENHANCED OIL RECOVERY FEASIBILITY EVALUATION FOR EAST TEXAS OIL FIELD

BY

PING LU

Submitted to the graduate degree program in Petroleum Engineering and the Graduate Faculty of the University of Kansas in partial fulfillment of the requirements for the degree of Master of Science

_____

Chairperson: Jenn-Tai Liang

_____

Jyun-Syung Tsau

_____

Russ Ostermann

Date Defended: 07-23-2012

The Thesis Committee for PING LU

certifies that this is the approved version of the following thesis:

CO2 ENHANCED OIL RECOVERY FEASIBILITY EVALUATION FOR EAST TEXAS OIL FIELD

Chairperson: Liang Jenn-Tai

Date approved: 07-24-2012

ABSTRACT

Carbon dioxide enhanced oil recovery (CO_2-EOR) has been undergoing for four decades and is now a proven technology. CO_2-EOR increases oil recovery, and in the meantime reduces the greenhouse gas emissions by capture CO_2 underground.

The objectives of this study are to improve the understanding of the mechanisms of CO_2 flooding, and to investigate the feasibility of CO_2-EOR in the East Texas Oil Field (ETOF) by conducting laboratory experiments. The laboratory experiments include phase behavior studies (such as slim tube tests and swelling/extraction tests) and core flooding tests.

Initial laboratory experiments indicated that miscibility was not achievable at current reservoir conditions and the oil recovery was low. Besides the low oil recovery, severe core plugging and decrease in injectivity were found throughout the experiments. ETOF was not a recommended candidate for CO_2-EOR currently. But further research could be done on developing new technology to reduce core plugging and well leaking, and finding more economically available CO_2 sources.

ACKNOWLEDGEMENTS

I owe my deepest gratitude to my supervisor, Professor Jenn-Tai Liang, for his guidance, encouragement and support throughout my study at the University of Kansas. He has always found ways to inspire me and provided ideas on improving my research, not to mention his financial support for the research and study.

I am sincerely and heartily thankful to my co-advisor, Dr. Jyun-Syung Tsau for his instructions in the lab, his ideas on experiments and thesis writing, and his patience with me. My thesis would not have been possible without his help.

I would like to show my gratitude to the Lab Director of our Tertiary Oil Recovery Group, Dr. Karen Peltier, for her instructions on lab safety and instrumental usage. I am very grateful to our lab technician, Mr. Scott Ramskill, for his assistance on setting up equipments.

It is a great pleasure to work with Tertiary Oil Recovery Group (TORP) members from whom I gained invaluable knowledge, experience and friendships.

I would like to acknowledge Research Partnership to Secure Energy for America (RPSEA) and the University of Kansas Center for Research's Tertiary Oil Recovery Project (TORP) for financial support.

I also want to thank Dr. Russ Ostermann for his efforts on my thesis writing and final defense.

Finally, to my family and friends, I owe all my heart for their love and support.

TABLE OF CONTENTS

1. INTRODUCTION AND LITERATURE REVIEW

Enhanced oil recovery (EOR) involves one or more of a variety of processes that seek to improve recovery of hydrocarbon from a reservoir after the primary production phase. EOR can be categorized mainly as chemical injection, gas injection, and thermal recovery. Gas injection, including natural gas injection, nitrogen or CO_2 injection, can either push out oil or thin it. Among these gas injection methods, CO_2 injection is considered the one of the most promising techniques.

1.1 Current Status of CO_2 Enhanced Oil Recovery (CO_2-EOR)

As the challenges of promoting enhanced energy security and in reducing greenhouse gas emissions grow, the concept of CO_2-EOR technology has received increasing attention. In fact, CO_2-EOR has been underway for 40 years, starting initially in the Permian Basin filled with uncertainties and developed to a proven technology with 114 CO_2-EOR projects currently installed in numerous regions of the USA today (Figure 1-1).

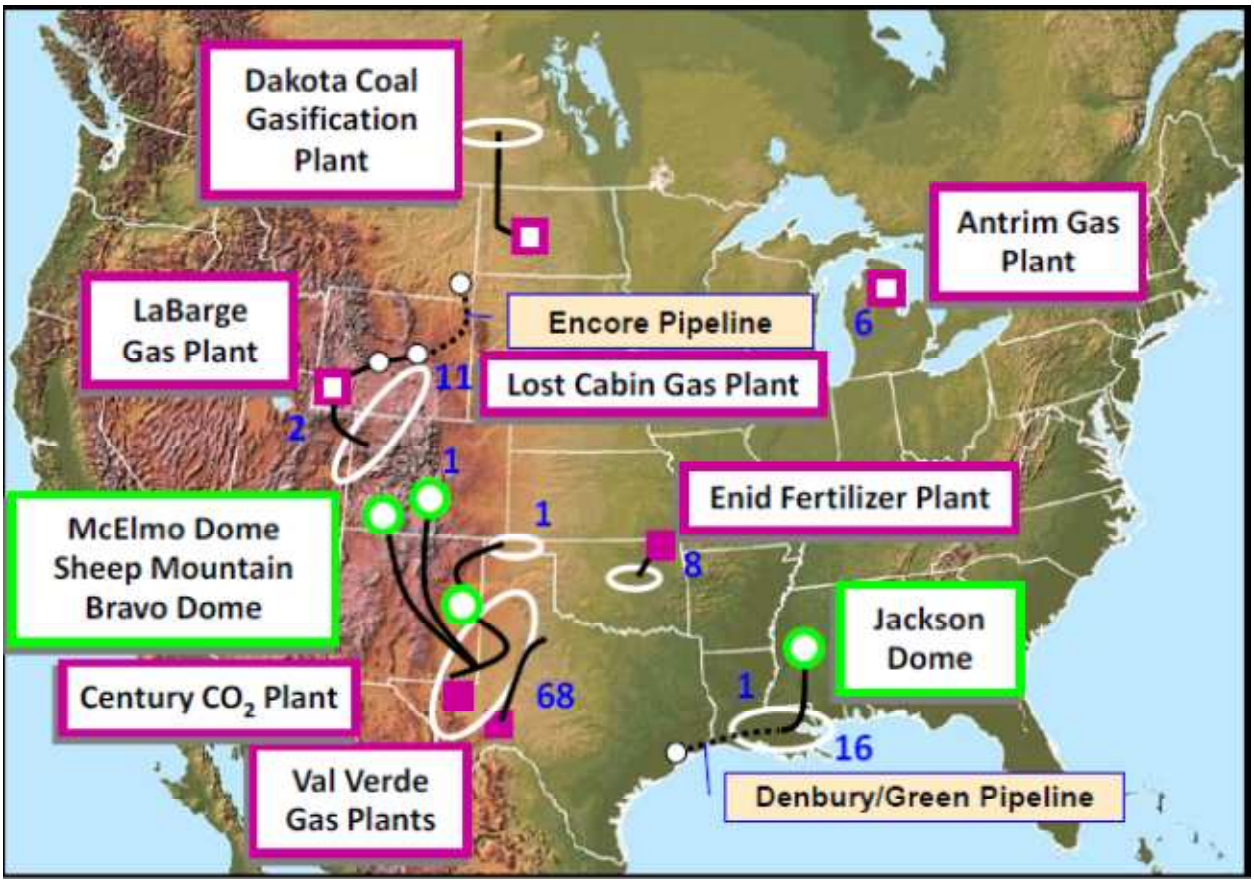

Figure 1-1 The current CO_2 EOR activity (Advanced resources international, Inc, March 2010)

"CO_2-EOR currently provides about 281, 000 barrels of oil per day in the U.S., equal to 6% of U.S. crude oil production" (Vello A. Kuuskraa et al, June 2011). As shown in Figure 1-2, between 1988 and 2008, oil production from CO_2-EOR grew five-fold in the U.S.

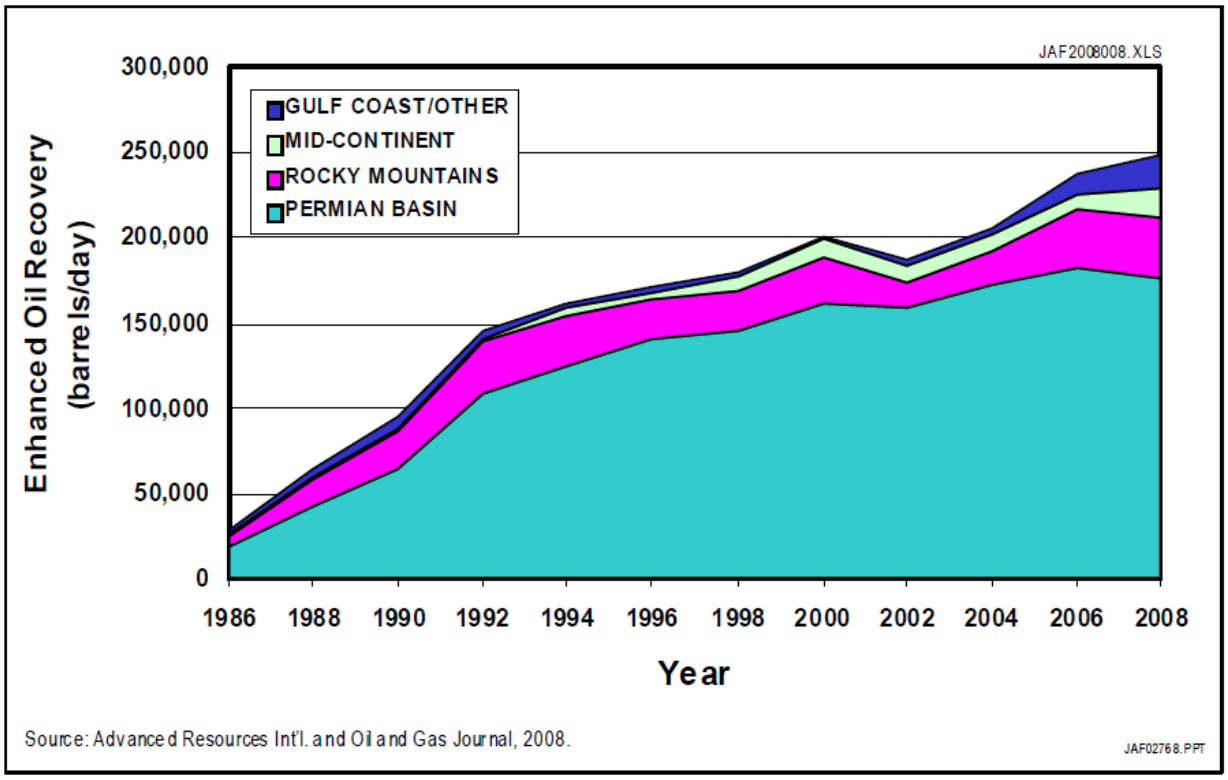

Figure 1-2. Growth of CO_2-EOR Production in the U.S. (1986-2008)

Today, the bulk of the CO_2 used for EOR comes from natural sources which are supplemented by modest, but growing, sources of anthropogenic CO_2. Still, the main barrier to reaching higher levels of CO_2-EOR production is a lack of access to adequate supplies of affordable CO_2 (Advanced resources international, Inc, March 2010).

The "Next Generation" CO_2-EOR technology would bring significant oil recovery and CO_2 storage far beyond those available from today's state of art (SOA) CO_2-EOR technology (Vello A. Kuuskraa et al, June 2011). Table 1-1 shows an estimation of economically recoverable domestic oil would increase to 67 billion barrels with "Next

generation" technology compared to 27 billion barrels with today's State of Art (SOA) technology.

Basin/Area	Technically Recoverable Oil (Billion Barrels)		Economically Recoverable Oil** (Billion Barrels)		Economic CO_2 Demand/Storage** (Million Metric Tons)	
	SOA	"Next Generation"	SOA**	"Next** Generation"	SOA**	"Next Generation"
1. Miscible CO2-EOR						
Lower-48 Onshore	55.7	104.4	24.3	60.3	8,940	17,230
Alaska	5.8	8.8	2.6	5.7	1,490	2,330
Offshore GOM	-	6.0	-	0.9	-	260
Sub-Total	61.5	119.1	26.9	67.0	10,430	19,820
2. New Miscible CO2-EOR	n/a	1.2	n/a	0.2	-	110
3. Residual Oil Zones	n/a	16.3	n/a	***	-	***
Total	61.5	136.6	26.9	67.2	10,430	19,930

JAF2011_030.XLS

*Includes 2.6 billion barrels already produced or placed into reserves with miscible CO_2-EOR and 2,300 million metric tons of CO_2 from natural sources and gas processing plants.

**At an oil price of $85 per barrel and a CO_2 cost of $40 per metric ton with ROR at 20% before tax.

***The economics of recovering oil from the residual oil zone were beyond study scope.

Table 1-1 Comparison of technically and economically recoverable domestic oil and CO_2 storage capacity from State of Art (SOA) and "Next Generation"CO_2-EOR technology (Vello A. Kuuskraa et al, June 2011)

Vello A. Kuuskraa et al stated that the "'Next generation' CO_2-EOR incorporates four significant and, with investments in R&D plus field pilots, realistically achievable advances in technology:

a) Improvements in currently practiced CO_2-EOR technology

b) Advanced near miscible CO_2-EOR technology

c) Application of CO_2-EOR to residual oil zones (ROZs)

d) Deployment of CO_2-EOR in offshore oil fields (Vello A. Kuuskraa et al, June 2011)."

1.2 CO_2 Properties

There are many properties that make CO_2-EOR a promising gas injection technique over others. First, CO_2 can extract heavier components up to C30 (Odd Magne Mathiassen, May 2003). Second, the pressure required for CO_2 becomes miscible with oil is generally substantially lower than others. Third, the high solubility of CO_2 in hydrocarbon oil causes the oil to swell. CO_2 expands oil to a greater extent than methane and nitrogen does. Fourth, CO_2 reduces oil viscosity and density. Fifth, CO_2 can vaporize and extract light components of the oil, reduce the surface tension of oil, and result in a more effective displacement. Last but not least, at high pressures, CO_2 density and viscosity are higher than those of other gases, which make CO_2 less prone to gravity segregation and more favorable in mobility control. Still, one of the main problems in achieving profitable CO_2 flooding has been the high mobility of the CO_2. The relative low density and viscosity of CO_2 compared to reservoir oil are responsible for gravity segregation and viscous fingering. In order to improve the sweep efficiency, several processes and methods can be done:

a) Alternating CO_2 and water injection (WAG)

b) Addition of foaming solutions together with CO_2

c) Installation of well packers and perforating techniques

d) Shutting in production wells to regulate flow

1.3 Mechanisms of Oil Displacement by CO_2

The displacement of oil by continuous CO_2 gas injection can be classified as multi-contact miscible process and immiscible displacement**.**

1.3.1 Miscibility

Miscibility occurs when two fluids mix in all proportions to form a single phase without an inter-phase (Don W. Green and G. Paul Willhite, 1998).

1.3.1.1 First-Contact Miscibility (FCM)

First Contact Miscibility (FCM) refers to a condition of two fluids that are miscible directly when first brought into contact at a given pressure and temperature. In reservoir gas flooding, the injected gas composition, oil composition, temperature and the injection pressure determine the condition of first-contact miscibility (Don W. Green and G. Paul Willhite, 1998).

1.3.1.2 Multi-Contact Miscibility (MCM)

Multi-contact miscible (MCM) processes occur at pressures above the minimum miscibility pressures (MMP) in which there are more interchange of components or mixing zones between the injected gas and the reservoir fluid.

There are generally two types of multi-contact miscibility: the vaporizing-gas process and the condensing process.

1.3.1.3 Vaporizing-gas

In the vaporizing-gas process, the injected fluid is generally a relatively lean gas. As the injected gas moves through the reservoir, the intermediate components in the oil are vaporized into the injected gas. Through multiple contacts with crude oil, the lean gas becomes enriched and eventually becomes miscible with the crude oil (Don W. Green and G. Paul Willhite, 1998).

1.3.1.4 Condensing

In the condensing process, the injected fluid generally contains larger amounts of intermediate-molecular-weight hydrocarbons. Reservoir oil near the injection well is enriched by contact with the injected fluid first put into the reservoir. Hydrocarbon components are condensed from the injected fluid into the oil, and the oil will eventually be sufficiently modified to a lighter composition to become miscible with additional injected fluid and a miscible displacement will occur (Don W. Green and G. Paul Willhite, 1998).

1.3.1.5 Combined Vaporizing and Condensing

CO_2 and most crude oil are not first contact miscible at normal reservoir temperature and pressure. However, miscibility develops through multi contact under proper conditions of pressure, temperature and composition.

In general, CO_2 displacement is a combined vaporizing and condensing mechanism. “Injected CO_2 displaces water, mixes with the oil and dissolves in it, and extracts hydrocarbons from the oil. When the CO_2 concentration in the crude oil in the inlet region exceeds the solubility of CO_2 in the oil, a CO_2-rich phase appears. Because the CO_2-rich phase has a viscosity close to that of

CO_2, the CO_2-rich phase flows more rapidly than the oil-rich phase, contacting fresh oil. Again, CO_2 dissolves into the fresh oil ahead of the front until the solubility of CO_2 has been reached. Eventually, the CO_2-rich phase contains enough extracted hydrocarbons to condense into the oil phase and bank up residual oil efficiently" (F.M. Orr Jr., April 1982).

1.3.2 Immiscible CO_2 Displacement Method

At pressures lower than MMP, CO_2 would dissolve in the oil and the oil expands, so the initially immobile residual oil becomes mobile due to oil swelling. IFT between CO_2 and the residual oil is not zero in immiscible CO_2 displacement, retaining the capillary pressure and resulting in lower oil recoveries compared to miscible displacement. In addition, CO_2 can reduce oil viscosity significantly which favors the mobility ratio. Also, CO_2 injection would maintain reservoir pressure (E. Tzimas et al, December 2005).

1.4 Geological Setting of This Study

East Texas oil field (ETOF) is located in East Texas Basin of eastern Texas, and it's on the west flank of the Sabine Uplift (Figure 1a) (F. P Wang, 2008). According to F. P Wang, two pilot areas (Figure 1b) were selected for studying the primary engineering, geological, and operational factors controlling recovery; for describing the detailed reservoir architecture; and for assessing operational strategies for future exploitation. This study was to evaluate the feasibility of CO_2

flooding in ETOF based on oil and reservoir core samples from the two pilot areas.

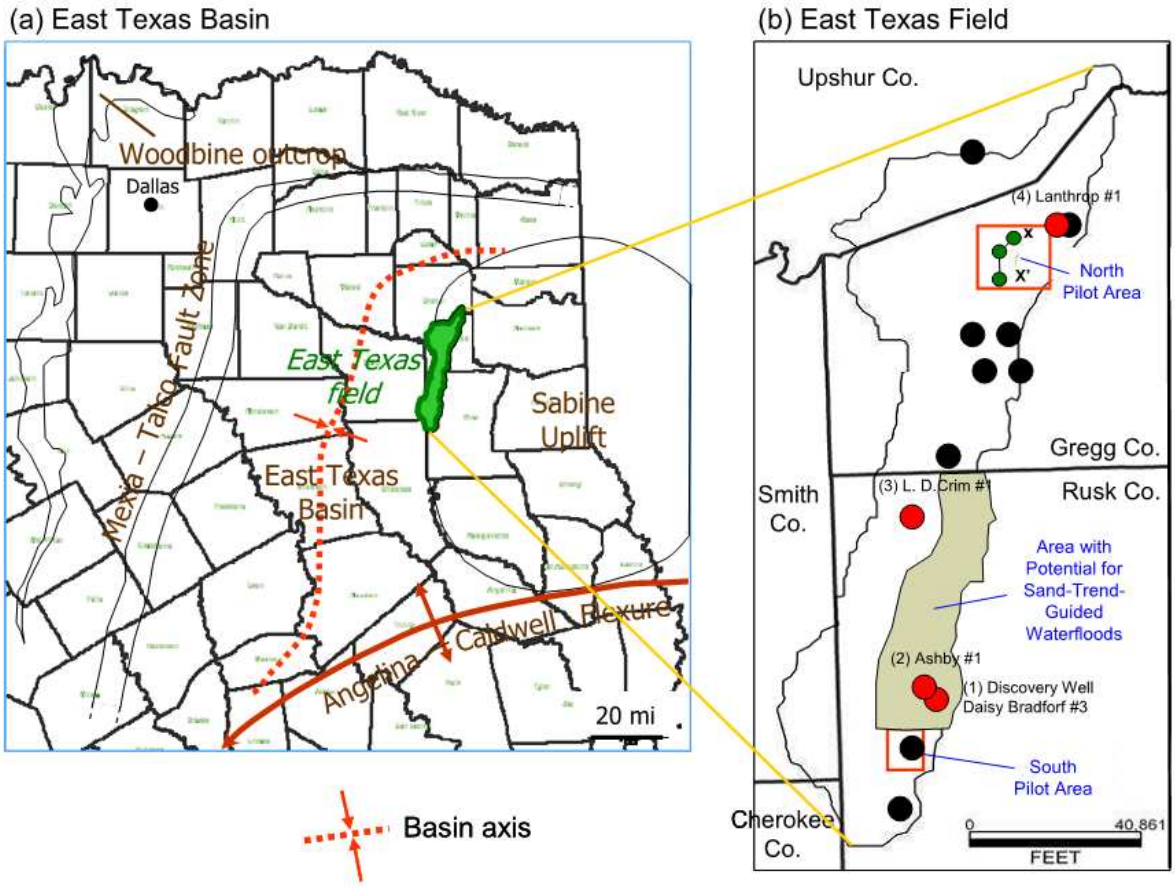

Figure 1-3 Location maps of (a) East Texas Basin and (b) East Texas oil field. Red circles represent the first four Producers; black circles are cored wells; squares represent the two study areas; and brown-colored area is the area with potential for depositional trend-guided water injection (F. P Wang, 2008)

ETOF is productive from the Upper Cretaceous lower Woodbine sandstone and is about 120ft thick (Figure 2). ETOF is bounded by the thin pre-Austin Chalk unconformity above, and the aquifer below. “Woodbine reservoirs in ETOF are composed of

predominantly non-marine sandstones, conglomerates and deltaic sandstones (F. P Wang et al, 2008)."

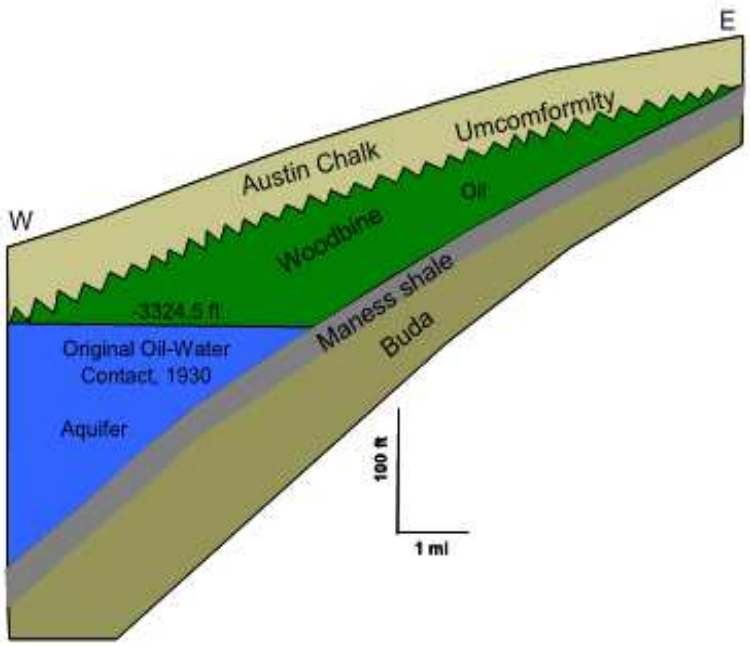

Figure 1-4 Wedge-type Stratigraphic Trap (F. P Wang)

Fluid and Reservoir Properties from literature can be summarized as:

Oil produced (BSTB)	5.42
Estimated OOIP midrange value (BSTB)	7.0
Current recovery efficiency	77%
Formation temperature (°F)	146
Oil gravity (API)	39
Oil viscosity (cP)	0.983
Porosity (%)	25.2

Permeability (mD)	2098
Initial water saturation (%)	14.1
Residual water saturation (%)	13.6
Saturation pressure (psia)	750
Formation volume factor (bbl/STB)	1.257
Solution Gas Ratio (scf/STB)	357
Formation volume salinity (ppm)	64,725

Table 1-2 Giant East Texas oil field fluid and reservoir properties (F. P Wang, 2008)

"The giant East Texas oil field's high recovery efficiency stems from its high reservoir quality, low residual oil, favorable stratigraphic dip, effective aquifer support, and stable water movement controlled by production rates" (F. P Wang, 2008). However, of the estimated 1.58 BSTB of remaining oil, only 70 MMSTB of remaining oil is likely to be produced under current operating techniques, and approximately 1.1 BSTB of residual oil will be produced under EOR methods (F. P Wang, 2008).

According to F. P Wang (F. P Wang, 2008), "with ETOF's 39° API oil at 146°F, minimum miscibility pressure for CO_2 is about 1850 psia. At a current reservoir pressure of 1,100 psia, CO_2 flooding would most likely be immiscible. Estimated recovery from immiscible CO_2 flooding is about 50% of miscible CO_2 flooding."

1.5 Objectives of This Study

1. Improve the understanding of the mechanisms of CO_2 flooding;
2. Investigate the feasibility of CO_2-EOR in the East Texas Oil Field.

2. PHASE BEHAVIOR STUDIES

2.1 Fluid Properties

In this study, all the East Texas Oil Field (ETOF) crude oil is filtered with Nylon cloth to remove any large size of grain particles likely in the oil, and then filtered through a filtering device at 35°C with one layer of 1.6um glass micro-fiber filter paper and another layer of 1um Teflon-laminated filter paper.

The compositional of crude oil was analyzed by Gas Chromatography (GC) technique and the results are shown below in Figure 2-1. It appears that filtration process does not affect the crude oil composition.

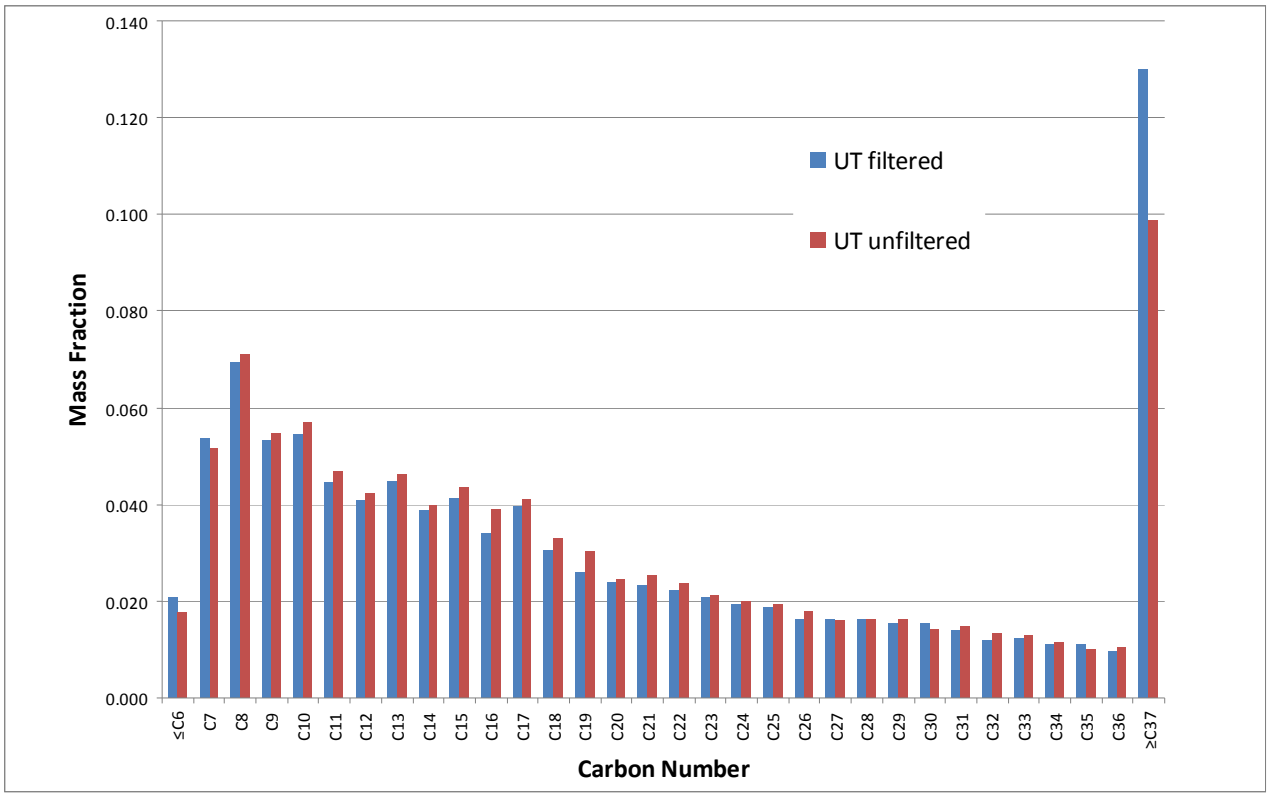

Figure 2-1 GC compositional analysis results of East Texas Oil Field (ETOF) crude oil

Physical properties of the filtered crude oil are listed in Table 2-1. The asphaltene content is determined to be 4% based on ASTM D 893-85 and will be discussed in detail in Chapter 3.

Molecular weight, g/mol	200.96
ETOF filtered oil viscosity at 63.3°C (cp)	1.95
ETOF filtered oil density at 25°C(g/cm3)	0.832
Asphaltene content by weight	4%

Table 2-1 Properties of filtered crude oil

Commercial CO_2 of 99.99% purity is used for CO_2 flooding.

2.2 Slim Tube Displacements

2.2.1 Purpose and Principle

The purpose of this slim tube experiment is to determine the minimum miscibility pressure (MMP). The MMP is the lowest pressure at which the injected gas and oil in place become multi-contact miscible. At this pressure, the displacement becomes very efficient. At pressures above it, very little additional recovery occurs.

There is no universally accepted method of defining MMP from slim-tube experiments. However, different methods generally yield results that are sufficiently close to each other for engineering purposes.

Some of the criteria of MMP are:

a) The pressure at which 90% of oil recovery reached at 1.2 HCPV of CO2 injected (Graig A. Williams et al, 1980).
b) The distinct point on the curve of oil recovery against flooding pressure (W. F.Yelling and R. S. Metcalfe, 1980).
c) The oil recovery reaches 80% at CO_2 breakthrough time (Shawket Ghedan, 2009).
d) The distinct point on the curve of oil recovery at gas breakthrough against pressure (Abiodun Matthew Amao et al, 2012).

In this study, MMP is defined as the pressure at which 90% of oil recovery reached at 1.2 HCPV of CO_2 injected as in criteria a), and the result is compared with MMP obtained from criteria b).

In a), oil recovery against pressure is plotted at 1.2 HCPV of CO_2 injected. MMP is obtained by drawing a line through 90% of oil recovery, and the corresponding pressure is MMP.

In b), oil recovery against pressure is plotted at 1.2 HCPV of CO_2 injected. The intersection of a line though the highest slope and a line through the nearly horizontal slope is the MMP.

2.2.2 Setup

Figure 2-2 shows the setup of the slim-tube test equipment. The slim tube consists of a stainless-steel tube that is 0.24 inches diameter and 38.29ft long. The tube is packed uniformly with glass beads of a size on the order of 100 meshes. The ratio of particle size to tubing diameter is sufficiently small that wall effects are negligible. The tube is coiled in a manner so that flow is basically horizontal and gravity effects are insignificant. The slim tube properties were evaluated by Rahmatabadi (Rahmatabadi and K. A., 2006) and listed in Table 2-1.

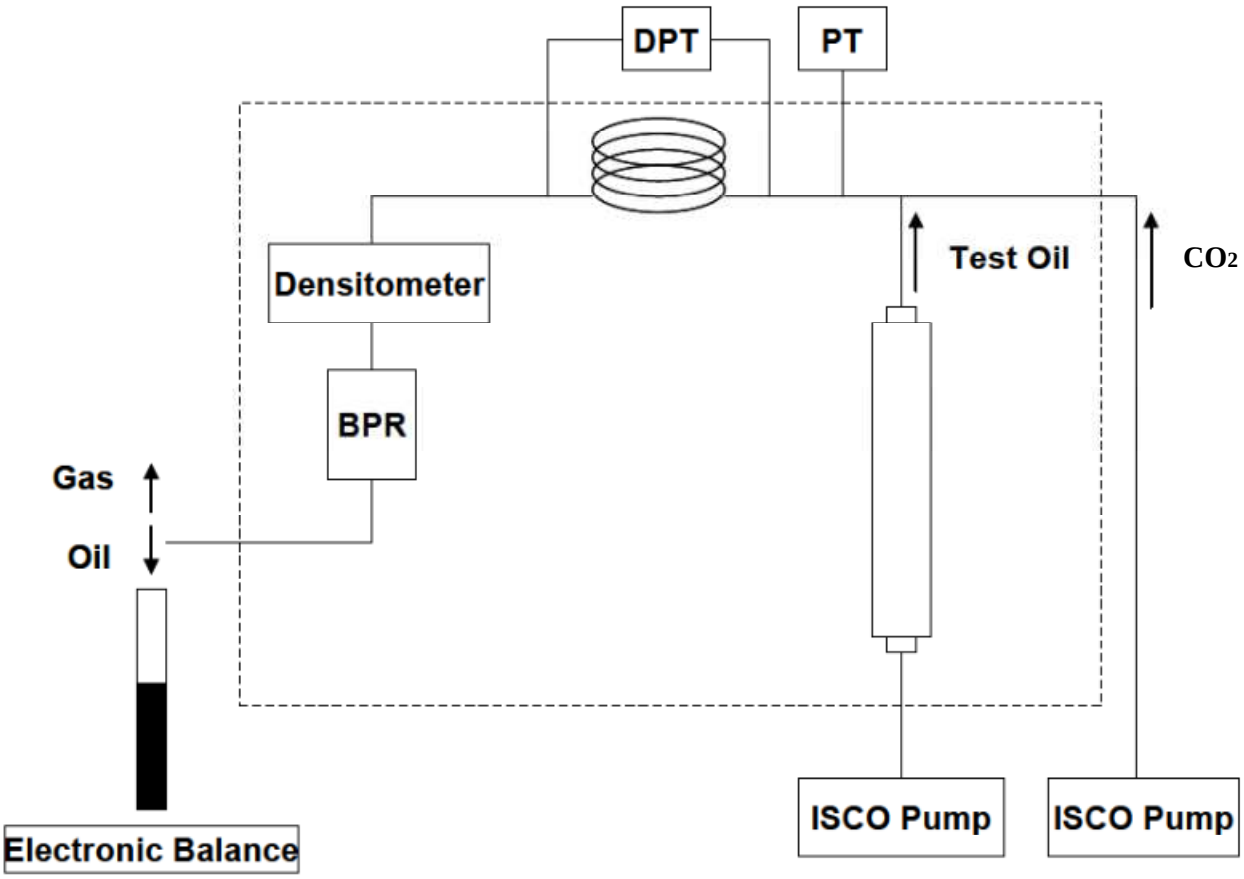

Figure 2-2 Slim tube setup [Ly Bui, 2010]

Length, ft	38.29
O.D, in	0.3125
I.D, in	0.2425
Porosity	0.367
Bulk Volume, cc	347.8
Pore Volume, cc	127.76
Permeability, mD	4900
Packing Beads	No.2024

Table 2-2 Slim tube properties [Rahmatabadi and K. A., 2006]

An injection system is provided to inject fluids into the slim tube. The injection system includes two syringe pumps (Isco, Inc. 260DM) for CO_2 and crude oil injection at desired rate, and one 485cc transfer cylinder for crude oil storage.

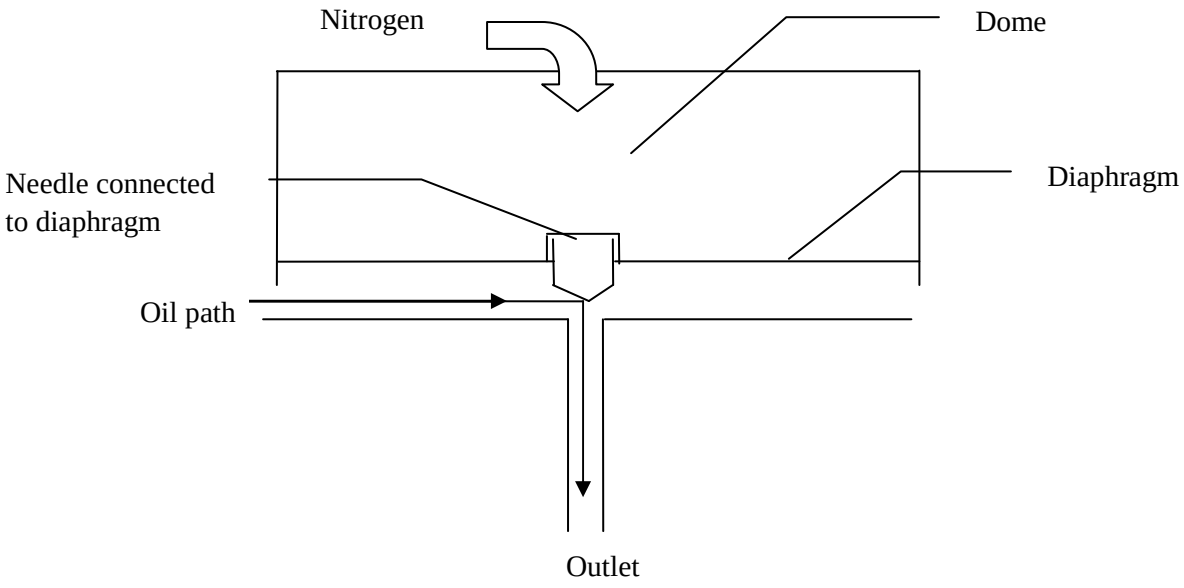

Figure 2-3 Schematic of the dome-load type back pressure regulator

The system pressure is controlled and maintained by a backpressure regulator (BPR) at the downstream of the slim tube. The model BPR-50 back pressure regulator is a dome-load type. It has a maximum operational pressure of 5000psi with a maximum temperature of 200°F. There is a diaphragm between the nitrogen dome and the outlet (Figure 2-3). A needle is connected to the diaphragm and points towards the outlet end. When the system pressure is in need of pressurizing, crude oil is injected through the system. Then the dome of the BPR is pressurized slowly by introducing high pressure nitrogen into the dome. When the dome pressure is higher than the downstream of the slim tube pressure, the needle connected to the diaphragm will be pushed by the diaphragm under pressure of nitrogen towards the outlet end and stop the fluids going through the BPR. As a result, the upstream fluids pressure will begin to catch up with the

BPR pressure until the upstream pressure is high enough that crude oil can flow through the BPR.

The slim tube, oil transfer cylinder, back pressure regulator and other auxiliary equipment are placed inside a Lindbergh/ Blue M oven with Eurotherm temperature controller. The temperature is set at a constant reservoir temperature of 146°F.

Oil pressure, CO_2 pressure, pressure drop across the slim-tube, and back-pressure regulator pressure are measured by four Valydine pressure transducers. The absolute pressure transducers have the capability of measuring pressures up to 2500 psi with the accuracy of 0.25% of their full scale (0-2500 psi) while the pressure range of the differential pressure transducer is 50 psi with the accuracy of 0.05% of its full scale.

The effluent end of the slim tube is exposed to atmospheric conditions. The separator gas is connected to a flow meter. The fluid is collected by a graduated cylinder which is on top of an electronic balance connected to the data acquisition system.

2.2.3 Procedure

To conduct a test, the porous medium in the tubing is filled with the crude oil to be displaced for at least 2PV. The system is brought to test temperature at 146°F, and the back-pressure regulator

is set at the desired displacement pressure. Once the desired pressure is reached, the system is allowed to equilibrate under pressure. CO_2 pump temperature is set by a circulator at the temperature of the system. CO_2 pump pressure is set slightly above the pressure of the back pressure regulator. CO_2 flow rate is set at a constant rate of 0.1cc/min.

A profile for the temperature of the system, pressure of the system, CO_2/oil pressure, pressure drop across the slim tube, weight of the separator liquid, and separator gas flow rate is created and set to be logged by the computer. The initial and final volumes of CO_2 in the pump are recorded manually.

For each displacement experiment, pumping of CO_2 is stopped after 1.2 HCPV of CO_2 is injected. Then the system is depressurized by venting the dome loaded gas slowly. Then the system is cleaned by injecting at least 10 PV of methlyene chloride followed by 10 PV of mineral oil. The entire experiment is repeated several times at different pressures, but with all other variables held constant. Recoveries are plotted as a function of displacement pressure.

2.2.4 Results and Discussions

Percentage of oil recovery was calculated as follows:

% Oil Recovery= Weight of Oil Produced / (Pore Volume*Oil Density)*100%.

Pore volume (PV) of CO_2 injected was calculated as follows:

PV of CO_2 Injected= Time* CO_2 Flow Rate/ Pore Volume.

The oil recovery histories at different CO_2 injection pressure are presented in Figure 2-4 where it shows that the recovery of oil at the end of CO_2 injection (1.2 PV) increases with the pressure.

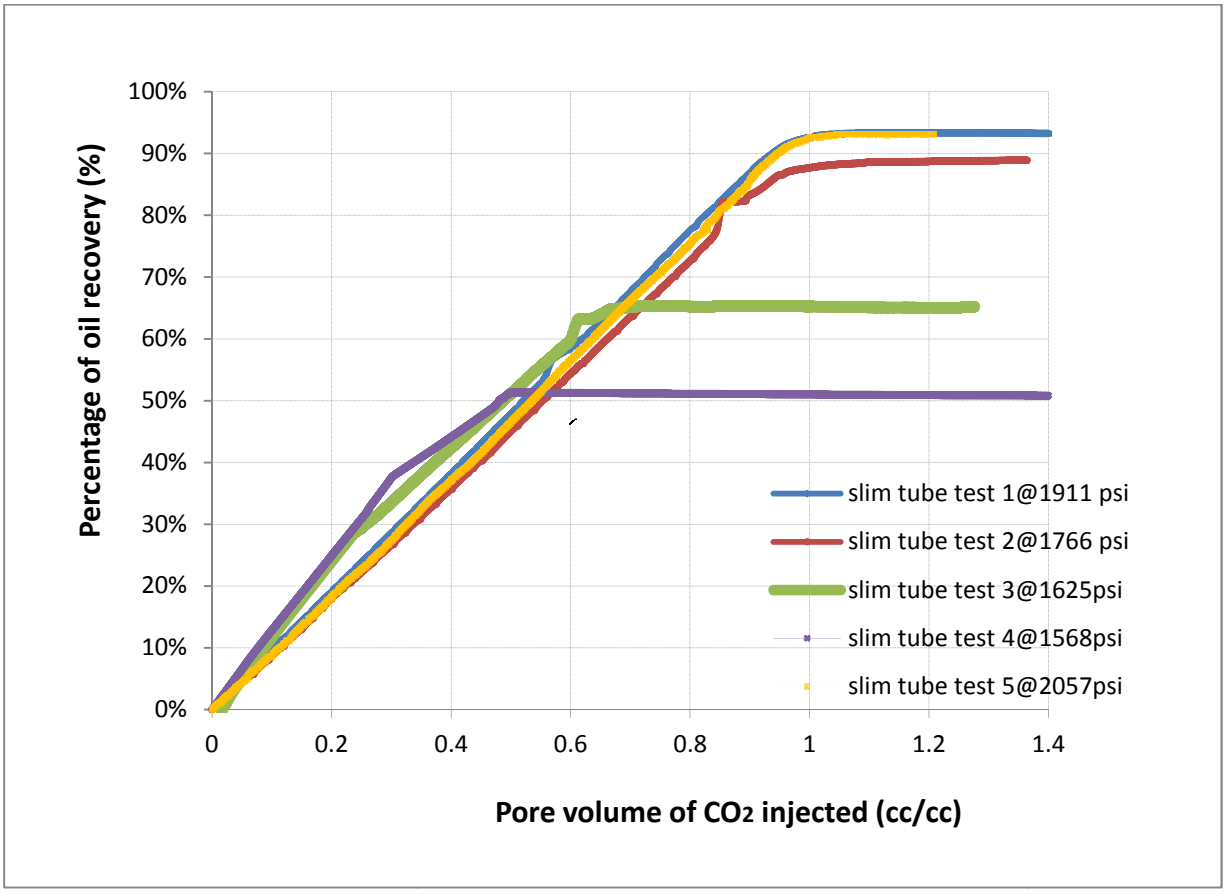

Figure 2-4 Results of slim-tube displacement tests at 146°F

Percentage of oil recovery at 1.2 PV of CO_2 injected was plotted against slim tube average pressure to determine the MMP of the system at 146°F, as shown in Figure 2-5. The MMP of the system was estimated to be 1776 psig at 146°F as the oil recovery at 1.2 PV of CO_2 injection reaches to above 90%.

MMP determined (as shown in Figure 2-6) from criteria a) is about 1776psi which is very close to 1780psi determined from criteria b).

Slim tube results indicated that miscibility was not achievable at the current reservoir pressure of 1100 psig.

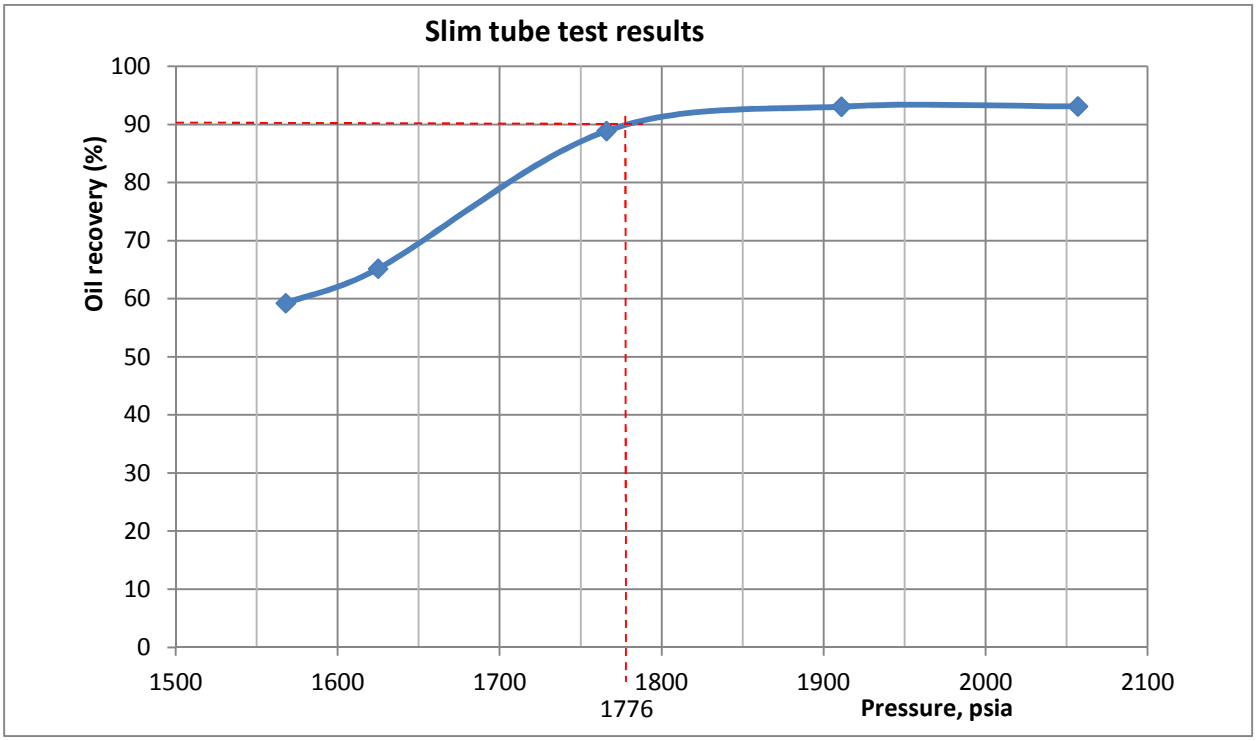

Figure 2-5 Slim tube tests for MMP determination from criteria a)

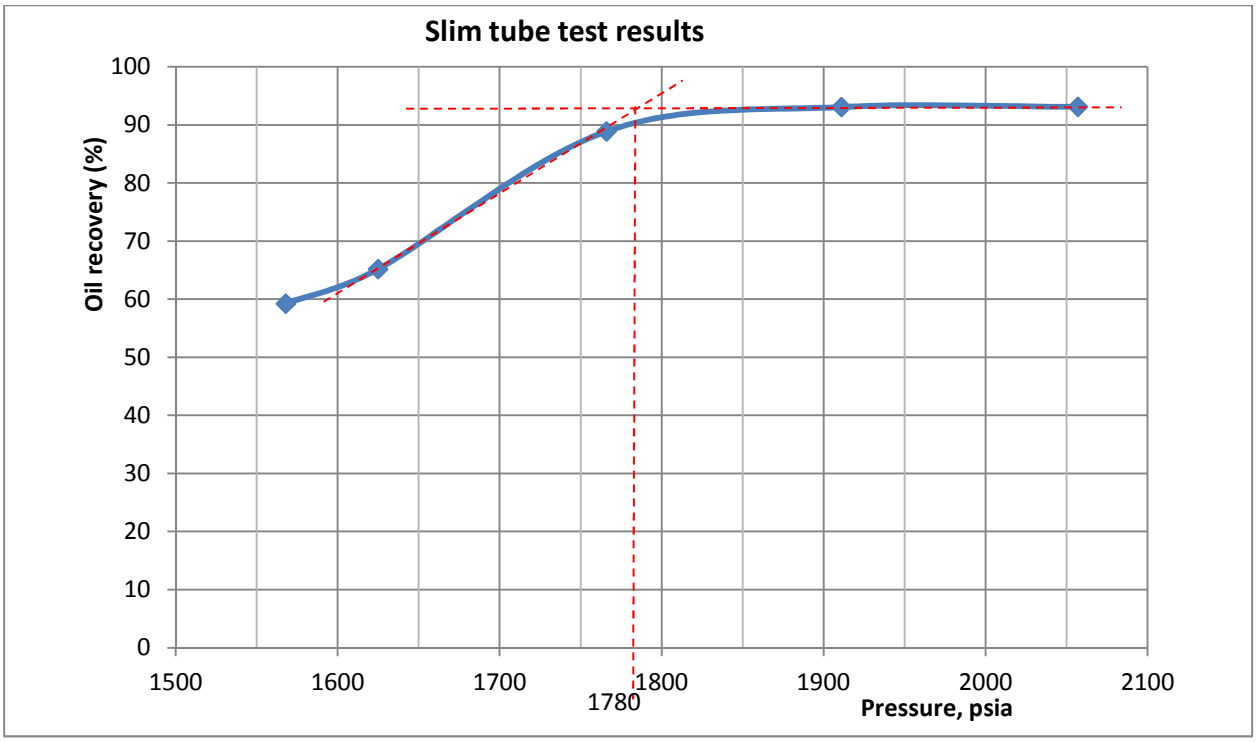

Figure 2-6 MMP determined from criteria b)

2.2.5 Conclusions

MMP was estimated to be 1776 at 146°F. Miscibility is therefore not achievable at the current reservoir pressure of 1100 psig.

2.3 Swelling/ Extraction Tests

2.3.1 Purpose

The purpose of swelling and extraction tests is to study the phase equilibrium behavior of the reservoir oil due to CO_2 dissolution and extraction, and to examine the oil recovery mechanisms with CO_2 injection. The saturation pressure, solubility of CO_2 and swelling factor are commonly measured in swelling test and used for tuning the equation of state (EOS) in modeling phase behavior. The phase behavior of ETOF crude oil and CO_2 at reservoir conditions is thoroughly studied through the swelling/extraction test.

2.3.2 Setup

The main components of apparatus are a high-pressure view cell, a high pressure and precision syringe pump filled with CO_2, a water bath, a cathetometer, and accessories to measure the temperature and pressure (Figure 2-7) (Ren et al, 2007).

The high-pressure equilibrium cell is equipped with a high-pressure gauge glass window allowing visual observation of the interaction between vapor and liquid phases with maximum pressure of 4000 psi and temperature of 280°C. The equilibrium cell consists of a rectangular vessel, which is fabricated out of stainless steel. A small PTFE coated stirring bar is placed inside of the cell. An external rare-earth magnet in a slot behind the cell enables the stir bar to mix throughout the cell.

A platform jack allows the water bath to be lowered away from the equilibrium cell or to be elevated to immerse the view cell. The temperature of the water bath is controlled by a Fisher Isotemp Immersion Circulator.

Pressure in the view cell is measured by a 5000psi Heise DXD Series 3711 precision digital pressure transducer.

The temperature of the ISCO 100DM syringe pump for CO_2 injection is controlled by a Fisher, Inc Isotemp circulator model 3016 and measured by an Ertco-Eutechnic 5 digital thermister model 4400. The gas lines are heated using fiberglass covered heating tape, controlled by two variable AC transformers, Staco Energy model 3PN1010B. The line temperatures are always maintained above the critical point of CO_2 (Tc=31.1 °C) at 60°C to eliminate CO_2 condensing. In order to prevent the heat from dissipating to the surroundings, a fiberglass cloth tape insulation is used. The line temperatures are measured by T-type thermocouples. An Eberbach 5160 cathetometer is used to measure the height of the liquid in the view cell.

The temperature of the lines, the pressure of the cell and the lines, the pump information including volume, flow rate, and pressure are monitored and logged by a computer using LABVIEW 8.2 software.

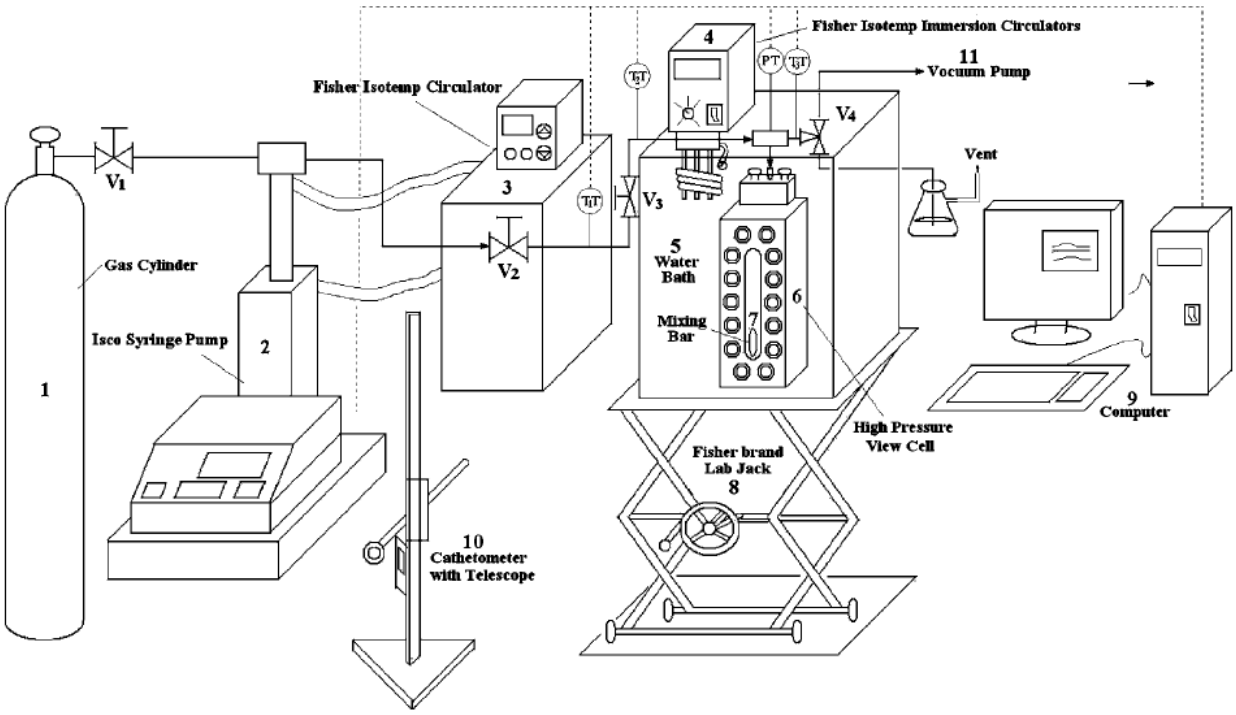

Figure 2-7 Diagram of experimental apparatus. (1) Gas cylinder; (2) syringe pump; (3) heater/circulator; (4) immersion heater/circulator; (5) water bath; (6) high-pressure view cell; (7) mixing bar; (8) laboratory jack; (9) computer; (10) cathetometer with telescope; (11) vacuum pump (Wei Ren, 2007)

2.3.3 Experimental Principle

The test is conducted in a constant volume, high pressure view cell initially filled with a predetermined amount of stock-tank oil. The pressure in the view cell is increased by injecting CO_2 into it at discrete steps. The change in the volume of crude oil due to the swelling is measured. In order to calculate the CO_2 solubility, the assumptions made in this study are that

a) The pressure of the compressed gas is much greater than the vapor pressure of the liquid.
b) Vaporization of crude oil components into the equilibrium vapor phase is negligible until the occurrence of significant extraction.

The phase equilibrium calculations are based on a CO_2 mass balance equation that state that the amount of CO_2 dissolved in the crude oil equals the total amount of CO_2 injected in the system subtracted by the amount of CO_2 increased in the lines and headspace above the liquid. The mass balance equation is

$$m_g = m_{pump} - (m_{lines} - m^0_{lines}) - (m_{headspace} - m^0_{headspace})$$

$$m_{pump} = \Delta V_{pump}\rho(T_{pump}, P_{pump})$$

$$m_{lines} = V_{lines}\rho(T_{lines}, P)$$

$$m^0_{lines} = V_{lines}\rho(T_{lines}, P^0)$$

$$m_{headspace} = (V_{cell} - V_l)\rho(T, P)$$

$$m^0_{headspace} = V_{headspace}\rho(T, P^0)$$

Where

m_g is the mass of CO_2 in the crude oil;

m_{pump} is the mass of CO_2 injected into the system, which is the product of the volume of CO_2 displaced by the metering pump (ΔV_{pump}) at constant temperature and pressure, and the density of CO_2 in the pump;

m_{lines} is the mass of CO_2 in the lines connecting the pump to the equilibrium cell. It is determined by multiplying the volume of the lines by the density of CO_2 in the lines;

$m_{headspace}$ is the mass of CO_2 in the headspace, which is calculated as the volume of CO_2 in the headspace multiplied by the density of CO_2 in the headspace. The volume of the headspace is the difference between the liquid volume V_l and the total cell volume V_{cell}. As the apparatus is purged with the compressed gas of interest to remove any air or other capping gases, some of the gas is initially in the lines and headspace;

m_{lines}^0 is the mass of CO_2 initially in the lines after venting the system; and

$m_{headspace}^0$ is the mass of CO_2 in the headspace initially in the system after venting.

CO_2 solubility in crude oil is defined as the mole fraction of CO_2 in the oil x_g.

$$x_g = \frac{n_g}{n_l + n_g} = \frac{m_g/M_g}{m_g/M_g + m_l/M_l}$$

Crude oil swelling factor is defined as the ratio of the final volume of crude oil after contact with CO_2 at a given pressure and the initial volume of crude oil at atmospheric condition.

CO_2 densities are determined from REFPRO database using ultraaccurate Span-Wagner equation of state (E. W. Lemmon et al, 2007).

2.3.4 Procedure

Figure 2-8 is a simplified sketch for illustration of experimental procedure.

1. Check the CO_2 pump to see if there is enough CO_2 in it. If not, refill the pump by connecting it to CO_2 cylinder and lowering the pump temperature.
2. After refilling the CO_2 pump, set the pump temperature at reservoir temperature 63.3°C. Set the pump pressure at constant pressure and above the maximum testing pressure, 2900psi in this case. The pump will automatically adjust the volume of CO_2 to achieve constant temperature and pressure.
3. Add enough water to the water bath tank. Set the water bath circulator temperature to reservoir temperature of 63.3°C.
4. Turn on the two alternating current transformers and set the temperature above the critical temperature of CO_2 at 60°C.
5. Check the view cell to make sure the bottom of it is sealed.
6. Place the view cell in the position of test.
7. Connect the mixing chain with the mixing bar in place.
8. Raise the laboratory jack to the point that the view cell is partially immersed into the water.
9. Use a syringe to get a 5cc sample of crude oil. Measure the total mass of liquid, syringe, and needle, and record it.
10. Inject the liquid vertically without splitting it on the wall.
11. Seal the top of the view cell quickly and make sure all the valves are closed.
12. Measure the total mass of syringe, needle, and the rest of the liquid, and record it.

13. Create a log file to record the pump temperature/ pressure/ volume, the view cell pressure/ temperature, and the temperature of gas lines.
14. When the system reaches equilibrium, flush the view cell with CO_2 at low pressure several times for venting the air:
    a. Close valves 2 and 3, and open valve1 slowly to make sure the pump pressure reaches about 3 bars.
    b. Close valve 1, open 3, and then open 2 slowly.

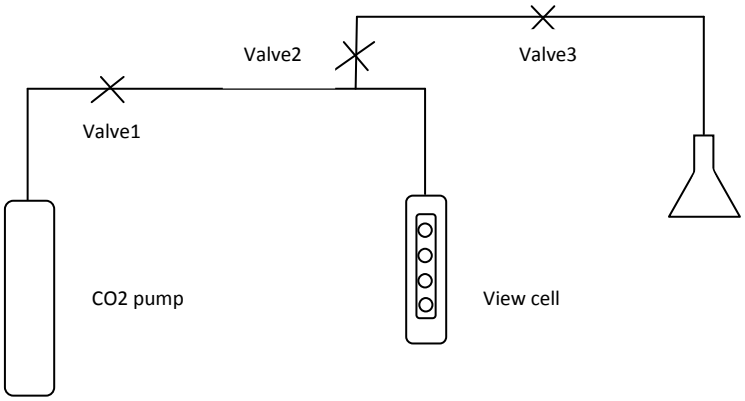

Figure 2-8 Simplified sketch of testing apparatus

15. Record the initial height of the liquid level, the pump temperature/ pressure/ volume, view cell temperature/ pressure, gas lines temperature.
16. Set the view cell pressure at desired pressure in discrete steps.
    a. If desired pressure is 20 bars, for example, open valve 1 slowly to about 30 bar, then close valve 1. Shake the mixing bar about 50 times to accelerate CO_2 dissolving into the crude oil.

b. When the pressure of the view cell does not drop much more, repeat step a. until the pressure is close to 20 bars.

c. Wait for a while until the pressure does not change much. Shake the mixing bar again about 50 times, if the pressure no longer changes, then stop and record the view cell liquid height, the pump pressure, temperature and volume, view cell pressure and temperature.

17. Record the final height of the liquid level, the pump temperature/ pressure/ volume, view cell temperature/ pressure, and gas lines temperature after each step.
18. Clean the view cell with methylene chloride followed by acetone solution, and blow dry.
19. A spreadsheet is developed to calculate the CO_2 solubility in the crude oil and swelling factor of the crude oil.

2.3.5 Apparatus Verification

This apparatus and method have been verified by Wei Ren (Wei Ren and Aaron M. Scurto, 2007) by comparing phase equilibrium data of CO_2 in n-decane at 71.1°C with published data.

2.3.6 Results and Discussions

Figure 2-9 shows the swelling/extraction curve for the crude oil/CO_2 system studied at 146°F with a sample size of 5cc. The swelling factor increases with the pressure as the dissolution of CO_2 in the oil increases. The swelling factor of this oil increases to 1.22 with maximum volume expansion of 22% when 0.67 mole fraction of CO_2 is dissolved in it at 1464 psig. After this point, as pressure further increases, light hydrocarbon components of crude oil are extracted into CO_2 rich phase and the oil shrinks and swelling factor decreases. The rate of extraction becomes

greater than swelling after 1464 psi. The composition of liquid phase after 1464 psi can no longer be determined from CO_2 material balance since the assumption that the liquid phase would not vaporize into CO_2 phase is not valid. The crude oil shrinks to 67.24% of its original volume at 2615 psi.

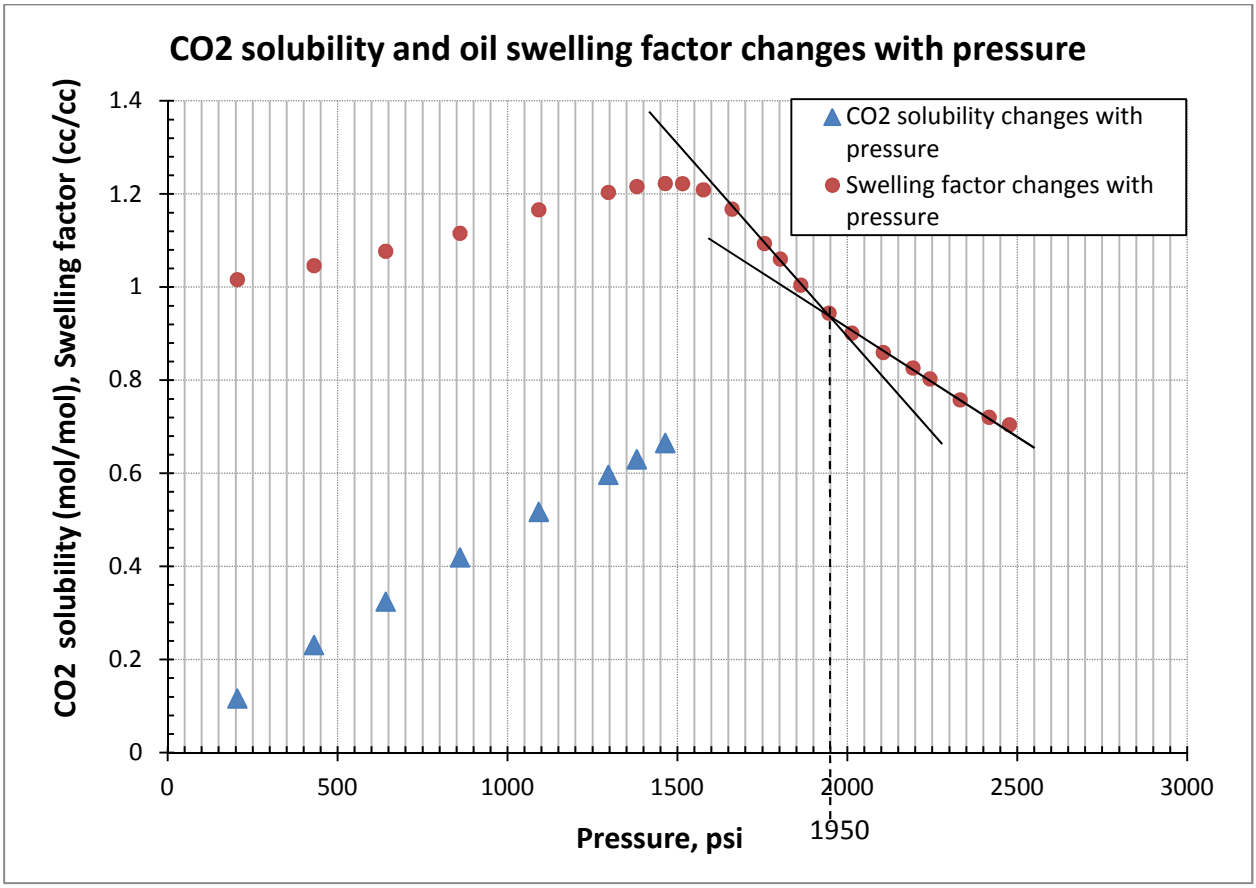

Figure 2-9 CO_2 solubility and oil swelling factor changes with pressure

J.S Tsau (J.S. Tsau, 2010) reported a relationship between the phase behavior observed in swelling/extraction tests and minimum miscibility pressure (MMP) determined from slim-tube

experiments. He observed that MMP can be graphically derived from the extraction test. According to him, the rate of slope changes in two distinct stages in extraction curve. “Drawing two lines through the major extraction and secondary stages, and the pressure at the intersection of these two lines is close to MMP determined with the slim-tube experiment.” Following this, as shown in Figure 2-8, the pressure at the intersection is 1950psi while MMP from slim tube is determined to be 1776psi.

Another study from Siagian (Siagian et al, 1998) shows that as there is a drastic increase in extraction capacity and density of CO_2-rich phase over a relatively small pressure range, the midpoint value would generally be a good MMP value to use. Following his observation, the oil extraction and slim tube results are compared in this study as shown in Figure 2-10. In the extraction test (Figure 2-10), the lower break and the upper break in the narrow pressure range of sharp change is 1520psi and 2020psi. The midpoint value is 1770psi, which is close to MMP of 1776psi from slim tube tests. Siagian (Siagian et al, 1998) also pointed out that “the fact that CO_2 MMPs are always within the range of pressures where efficient CO_2-oil extraction started, confirmed that extraction is a major process responsible for the development of CO_2-oil miscibility”.

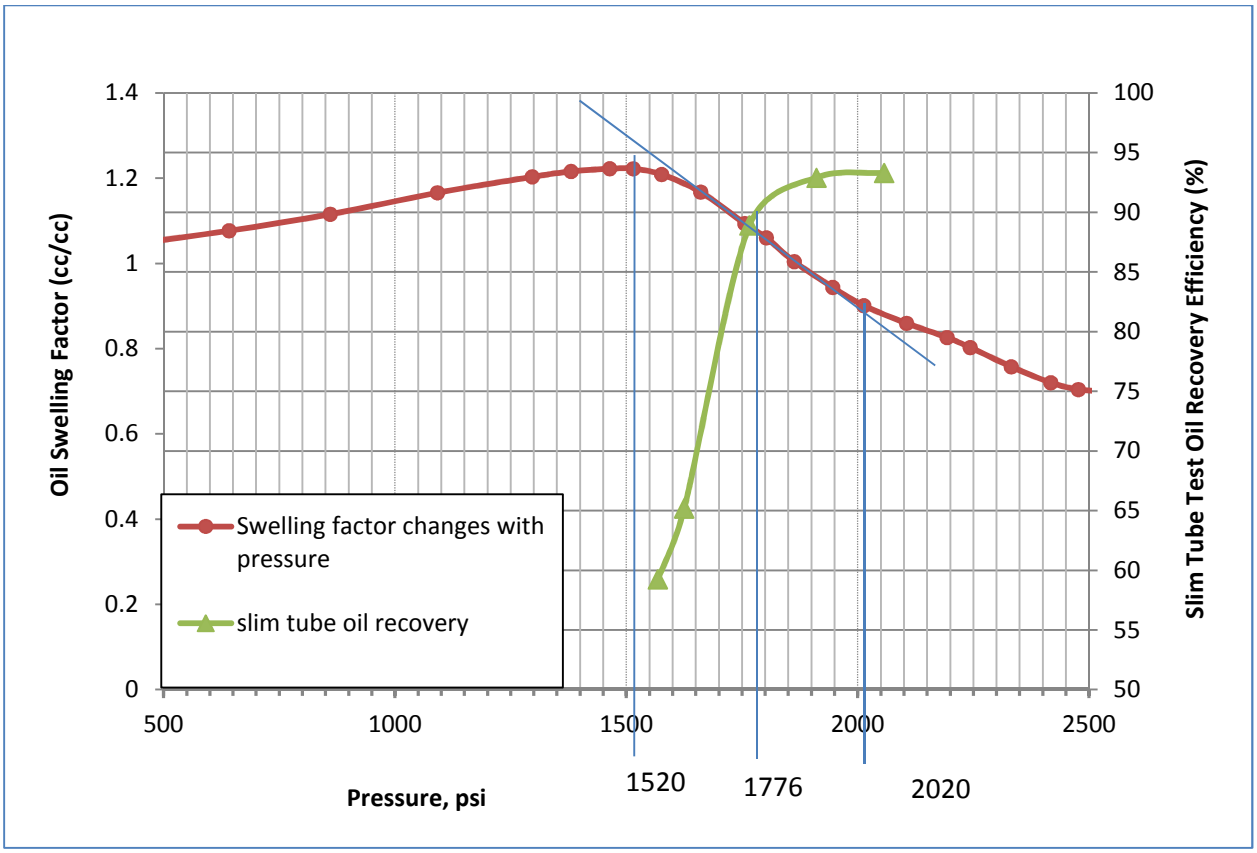

Figure 2-10 Illustration of relationship between CO_2 extraction test and slim tube MMP

2.3.7 Conclusions

1. At pressures below 1464psi, CO_2 solubility and oil swelling factor increase with increasing pressure as CO_2 dissolves in the oil and the oil expands.
2. Significant extraction starts at 1464 psi. The swelling factor decreases as pressure further increases after this point.
3. Extraction or vaporization of hydrocarbons is the principal mechanism of the multi-contact miscibility development.

2.4 Oil viscosity and oil/CO_2 mixture viscosity measurements

2.4.1 Purpose and Principle of Operation

Oil viscosity and oil/CO_2 mixture viscosity measurements are part of the basic phase behavior study of CO_2 enhanced oil recovery project. It shows the impact of CO_2 dissolution in the crude oil on the oil viscosity which would affect the oil recovery efficiency and it's useful for tuning the phase behavior model. A Cambridge Applied System high pressure viscometer is used in this study to measure viscosity.

2.4.2 Experimental setup and Specifications

The Cambridge Applied Systems piston-style viscometer (Figure 2-11) contains two magnetic coils inside a stainless steel body. A low mass stainless steel piston inside the measurement chamber is magnetically forced back and forth in the fluid. The time required for the piston to move a fixed distance (about 0.2 inches) is then very accurately related to the viscosity of the fluid in the chamber using the principles of annular flow around an axially oscillating piston (R.B. Bird, W.E. Stewart, E.N. Lightfoot, 1960). As the piston is pulled toward the bottom of the measurement chamber, it forces the fluid at the bottom of the chamber to flow around the piston toward the sensor opening where it interchanges with the normal flow of the fluid. On the upward piston stroke, fresh process fluid is pulled around the piston to the bottom of the measurement chamber. The flow deflector continuously diverts fluid from the process stream into the outer portion of the measurement chamber, thereby refreshing the measured fluid. Since measurement of the motion is made in two directions, variations in travel time due to vibration, orientation, and flow are almost completely eliminated. Temperature is measured continuously

with the use of a Resistance Temperature Detector (RTD) mounted at the base of the measurement chamber. Since the viscosity of a fluid varies significantly with temperature, it is important to know the exact temperature of the measurement chamber.

The sensor measurement range is 0.2 to 10,000 cp at a maximum pressure of 137.9 MPa and within a temperature range of 233.15K to 463.15K .The measurement chamber of the high pressure sensor is connected to a rupture disk and a precision pressure transducer.

The accuracy of this viscometer was validated earlier by Ahosseini et al. (Azita Ahosseini and Aaron M. Scurto, 2008), first by using standard calibration solutions, and then by comparing viscosity values of n-hexane measured using this viscometer with literature values. The uncertainty of this instrument is ±3%. The uncertainty of temperature is ±0.1K.

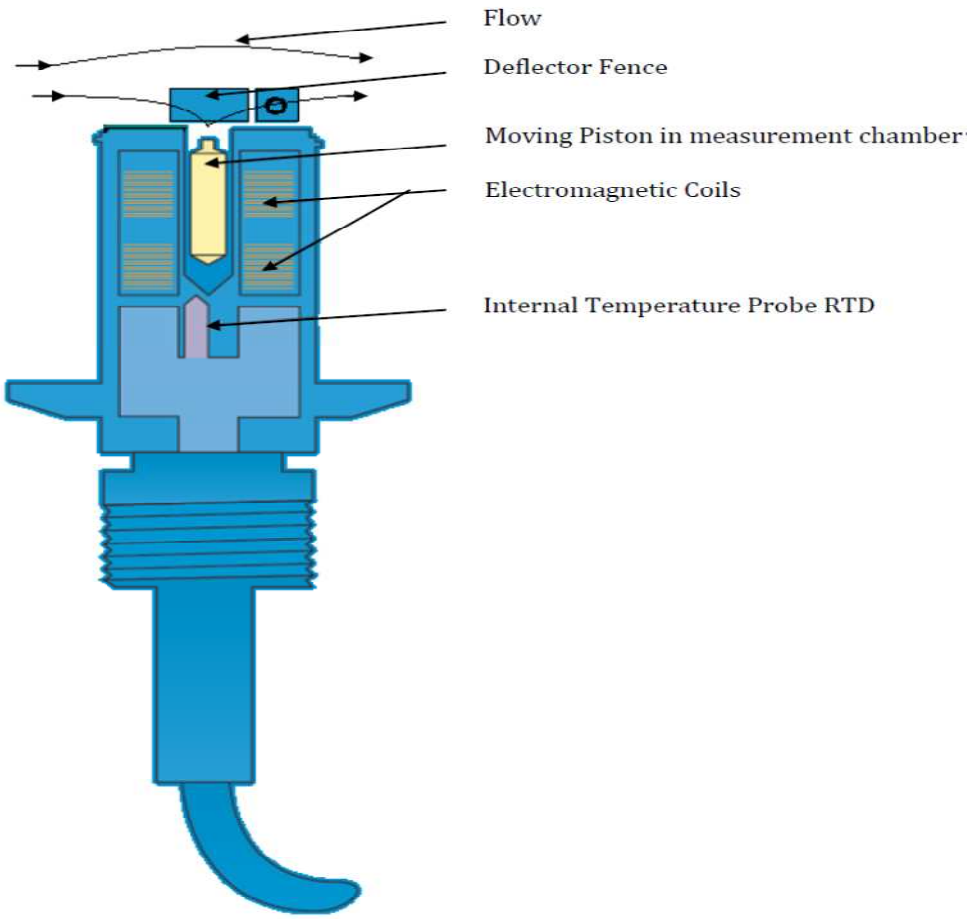

Figure 2-11 Cutaway view of sensor tip installed in a pipe line (ViscoPro 2000 Viscometer System Operations Manual, Cambridge Viscosity)

The schematic of the setup is shown in Figure 2-11. The high pressure sensor is placed inside a temperature-controlled oven together with a high pressure view cell and a densitometer, and is connected to a high pressure generator served as a pump for oil injection.

When the setup is used for viscosity measurements of crude oil/CO_2 mixture, the pressure of the system is increased by CO_2 injection. ISCO 260D pump- Model 1020BBB-4 is used for CO_2 transfer/injection. The view cell placed inside the oven allows observations of crude oil/CO_2 interaction. During pressurization process, the time required for the contents in the system to equilibrate under a particular pressure and temperature is minimized by a circulation pump- Micropump, Inc. Model 415A.

2.4.3 Procedure

2.4.3.1 Oil Viscosity Measurement Procedure

When the setup is used for oil viscosity measurement, the system fluid flow path follows the green line in Figure 2-12.

Temperature of the oven is set constant at reservoir temperature of 146°F. The handle of the high-pressure generator is rotated counter-clockwise to draw crude oil into the cylinder body. By rotating the high pressure generator handle clockwise slowly, the piston will compress the fluid to develop increased pressure in the system. When the system is at thermal equilibrium, the system is purged to dislodge any potential bubbles. The viscometer is turned off during pressurization process to avoid damaging. The system pressure is increased in discrete steps at about every 300psi interval.

After pressurization, viscosity reading is recorded three times when temperature and pressure of the system is stabilized approximately 20 minutes after pressurization.

2.4.3.2 CO_2/Oil Mixture Viscosity Measurement Procedure

When the setup is used for oil viscosity measurement, the system fluid flow path follows the orange line in Figure 2-12.

Temperature of the oven and ISCO pump is set constant at reservoir temperature of 146°F. Pressure of the pump was set constant at the maximum anticipated pressure 2100psi. Crude oil is injected into the measurement chamber and into the view cell. When the system is at thermal equilibrium, the system is purged to dislodge any potential bubbles. The system pressure is increased in discrete steps by CO_2 injection from the top of the view cell. The pressure interval is 200psi. CO_2 injection is stopped when a desired pressure is achieved. After each pressurization process, a micro-pump is turned on to circulate the liquid inside the system to help accelerate the mass transfer of the gas phase into the liquid phase. When the system temperature and pressure are stabilized one hour later, the viscometer is turned on and viscosity and density data is recorded.

In this study, only the viscosity at 63.1°C is measured. After turning on the viscometer for about 5 minutes, the measurement chamber temperature could increase to 63.2 due to the moving of

piston. This small increase of temperature could change the viscosity more significantly than the pressure increase.

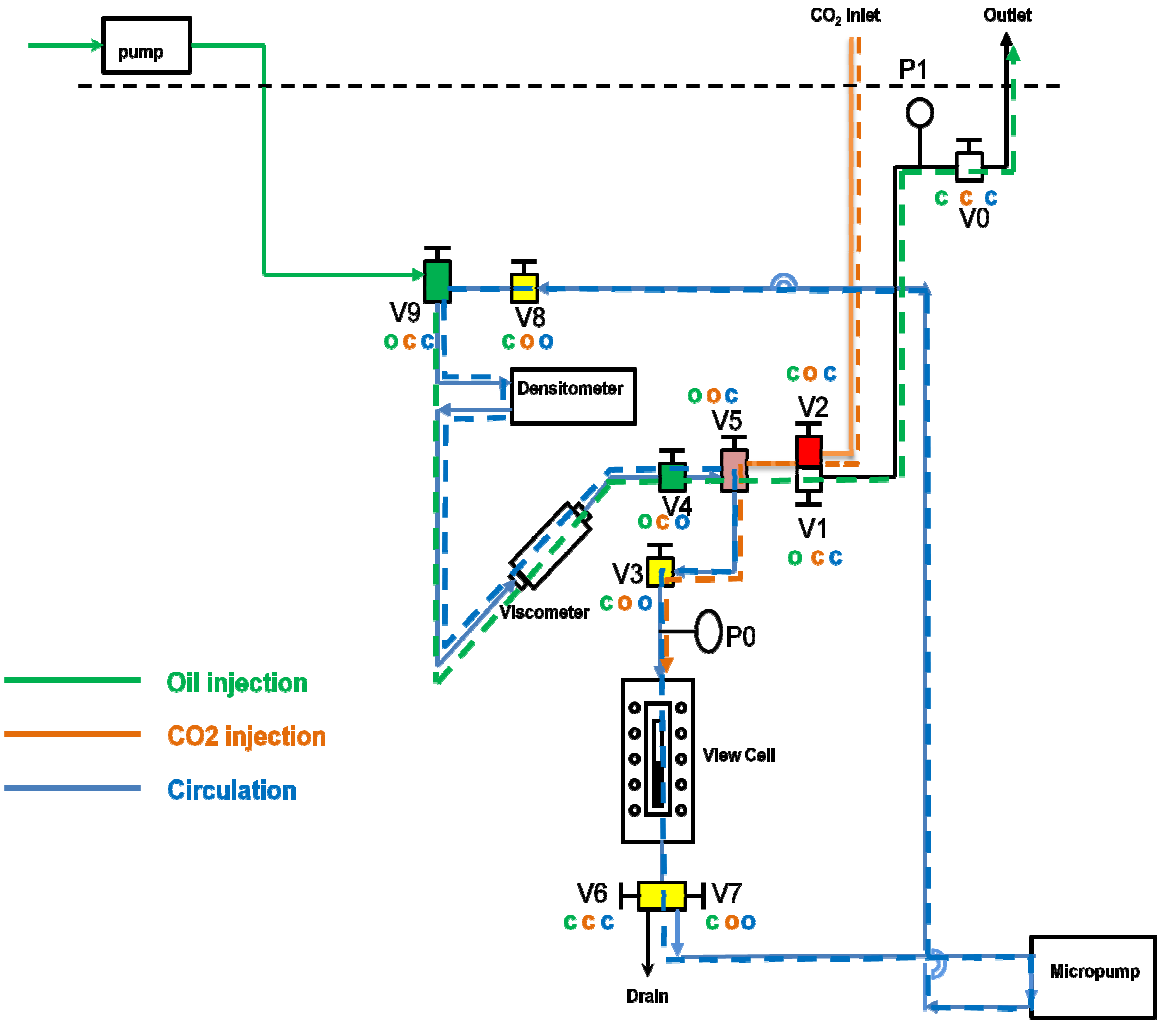

Figure 2-12 Schematic of the viscosity measurements setup ("o" represents the valve being open and "c" means keeping the valve closed)

2.4.4 Results and Discussions

Figure 2-13 demonstrates the viscosity of pure crude oil changes with pressure at 146°F. Pure crude oil viscosity increases with increasing pressure.

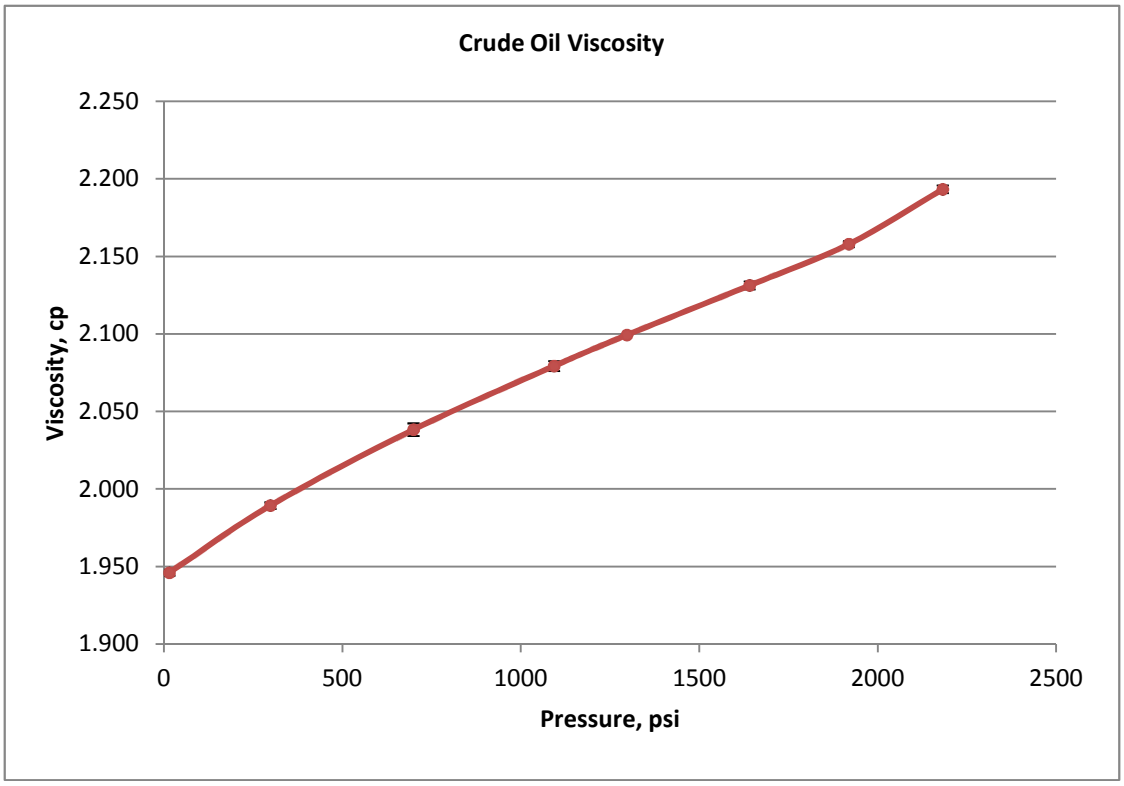

Figure 2-13 Effect of pressure on crude oil viscosity

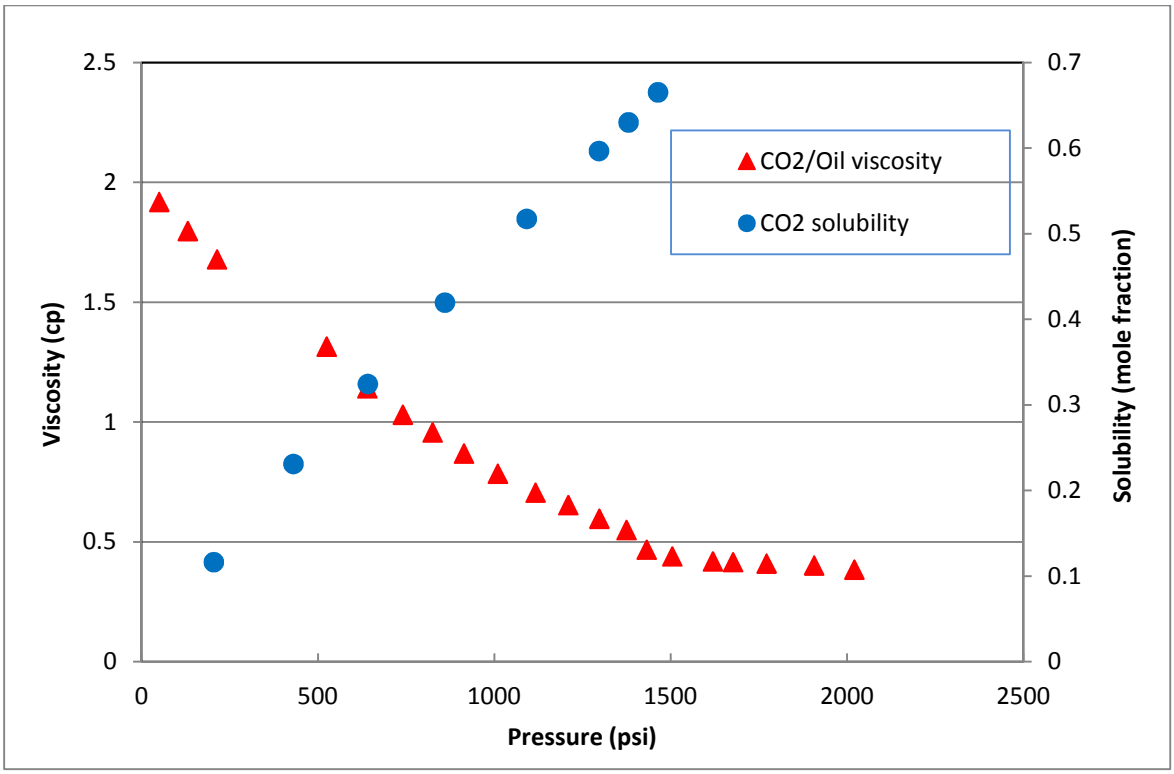

Figure 2-14 Effect of CO_2 dissolution in crude oil on the crude oil viscosity

Figure 2-14 shows the effect of CO_2 dissolution into the crude oil on the viscosity of crude oil at 146°F. In Figure 2-14, the CO_2 solubility is obtained from the swelling and extraction test previously. As CO_2 dissolves in the crude oil, viscosity of the crude oil is reduced by a factor of 5. At pressures above 1500psi, the effect of CO_2 on oil viscosity is minimal.

Figure 2-15 shows pure crude oil density. Crude oil density increases with increasing pressure.

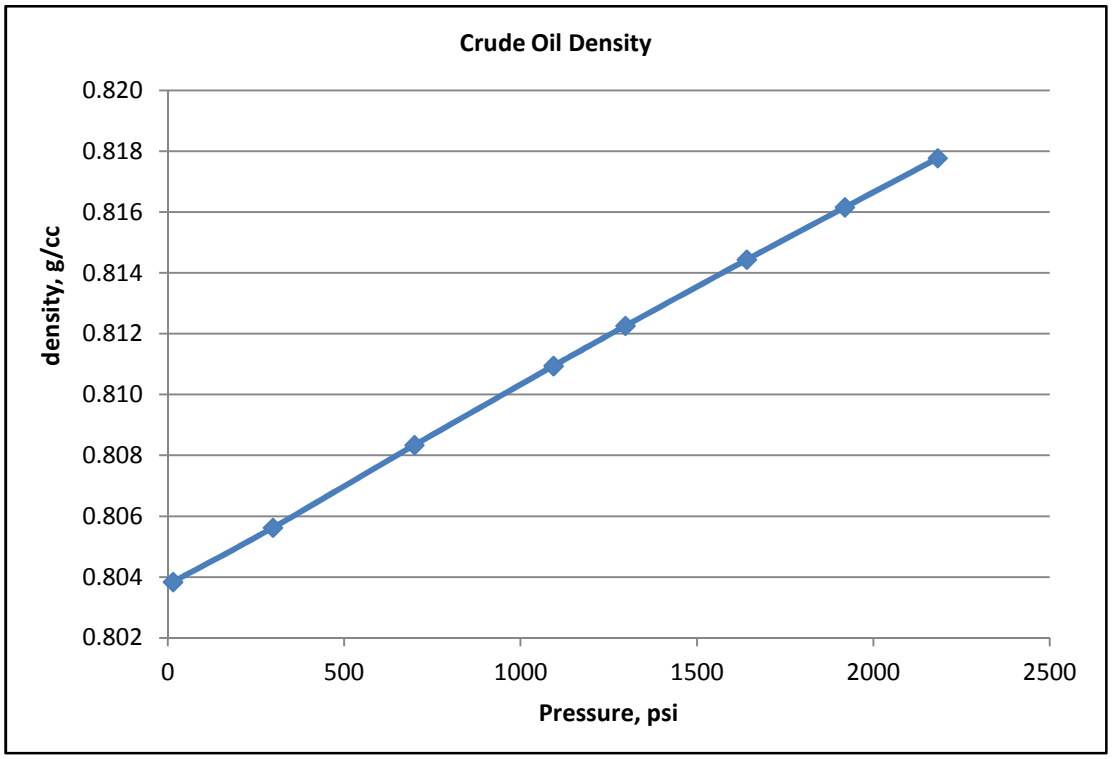

Figure 2-15 Crude oil density

Figure 2-16 shows the comparison of pure crude oil density and crude oil and CO_2 mixture density. The effect of CO_2 dissolution in crude oil on the crude oil density is minimal.

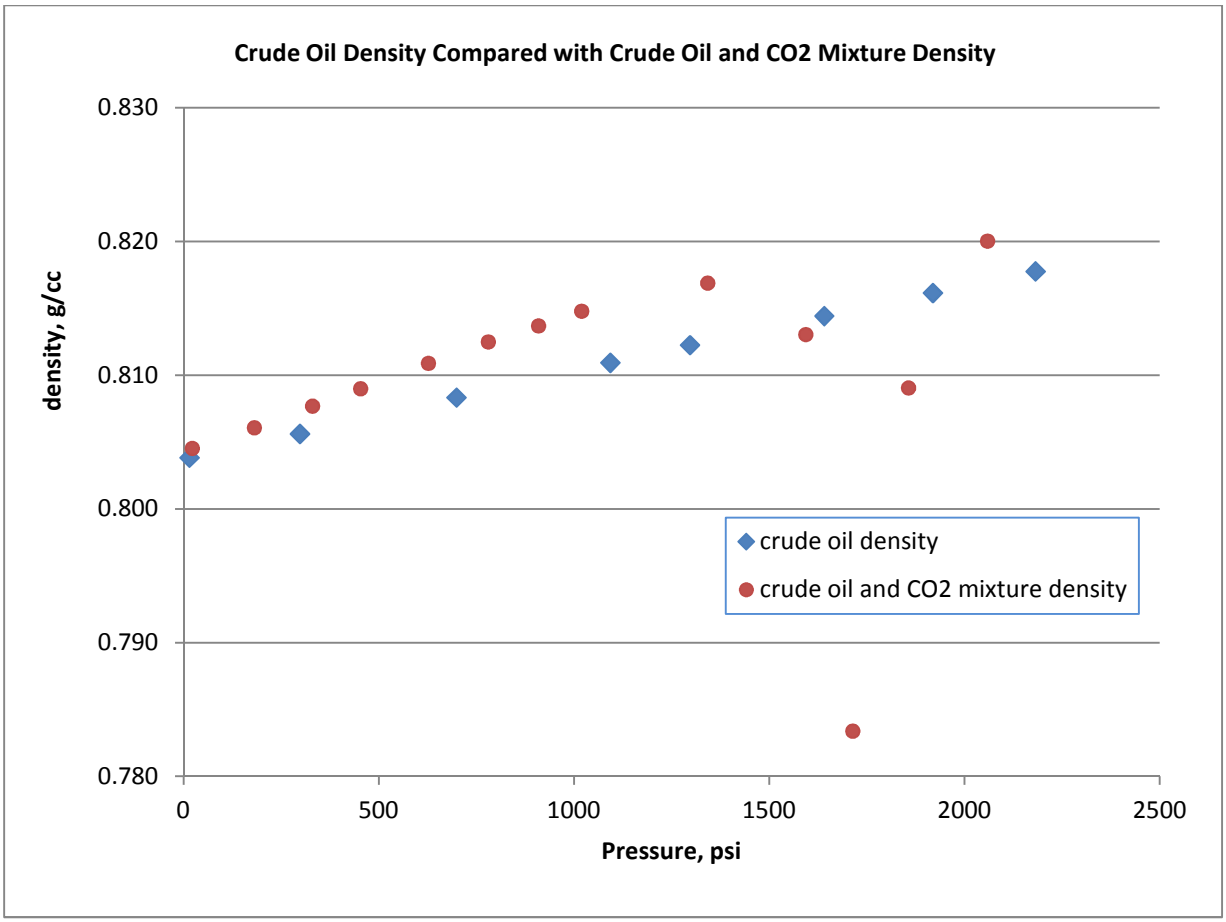

Figure 2-16 Effect of CO2 dissolution in crude oil on the crude oil density

2.4.5 Conclusions

1. A six-fold reduction in oil viscosity is achieved in the near miscible region 1500psi to 2000psi.
2. The reduction of oil viscosity improves the total mobility ratio between reservoir oil and the displacing fluid, which will be favorable to oil recovery efficiency.
3. Viscosity measurements are useful in tuning the phase behavior model.
4. CO_2 dissolution has little effect on the crude oil density.

3. CORE FLOW TESTS

CO_2 core flooding does not eliminate effects such as viscous fingering, gravity segregation, channeling or bypassing of oil. However, core flooding tests can:

a) Be more representative of the reservoir process and displace oil under conditions that are more realistic than in slim tubes;

b) Provide an opportunity to collect effluent samples from which compositions, densities, and viscosities can be determined, and all these data can be compared with simulator predictions (F.M. Orr Jr. et al, April 1982);

c) Address the influence of residual oil saturation, ROS, rock type, and reservoir drive;

d) Determine the tendency for asphaltenes to precipitate;

e) Define the ultimate potential of using CO_2 to improve oil recovery (Shawket Ghedan, 2009).

The purpose of core floods has always targeted the understanding of the displacement mechanisms rather than the measurements designed for use in scale-up calculations for particular reservoirs.

3.1 Core Sample Preparation

Reservoir heterogeneity effect is more pronounced in CO_2 flood than water flood due to high CO_2 mobility. Accurate reservoir characterization in any laboratory technical evaluation is

important to estimate volumetric sweep efficiency which would affect the CO_2 utilization factor (Shawket Ghedan, 2009). Fawas M. Al-Otaibi (Fawas M. Al-Otaibi et al, April 2012) suggests that the core flooding procedure should start with selecting a large number of core plugs for screening using computerized tomography (CT) scan and nuclear magnetic resonance (NMR) measurements. The CT scan is to make sure that there is no fracture or permeability barrier within the plugs. The NMR is to determine the micro and macro porosity distribution and ensure that the composite core plugs are of the same rock type.

In this study, Berea sandstone cores and East Texas Oil Field (ETOF) reservoir cores are used for comparison. The dimensions of the cores are measured. Each core is about one-inch in diameter and three-inches long. Then each core is encased with epoxy and cast inside an aluminum cylinder. The dry weight of the cores with core holder is measured.

Before each core flow test, the cores are cleaned with at least 10 pore volume of methylene chloride followed by 10 pore volume of methanol until the effluent fluid is clear. Then the cores are saturated with synthetic field brine.

3.2 Fluids preparation

The synthesized brine is prepared based on reservoir brine formulation, and the detailed formulations are listed below.

Salt	Chemical in wt% in synthesized brine
$FeCl_3.6H_2O$	0.01%
NaCl	5.77%
$CaCl_2.2H_2O$	0.50%
$MgCl_2.6H_2O$	0.45%
$NaHCO_3$	0.08%
Na_2SO_4	0.03%
Total Cl^-	3.90%

Table 3-1 Synthetic field brine composition

After filtering the brine with 0.45um filter paper, the properties of the synthesized brine were measured and shown below.

	Measured value
pH Value	7.05
Equivalent NaCl Conc. (%)	6.23
viscosity @ 25°C (cp)	1.09
viscosity @ 63°C (cp)	0.60
Density @ 25°C (g/cm3)	1.044
Density @ 63°C (g/cm3)	1.020

Table 3-2 Synthetic field brine properties

3.3 Equipments and Procedures

3.3.1 Core Characterization

Core characterization includes determining pore volume, porosity and permeability for each core.

3.3.1.1 Pore Volume Measurements

3.3.1.1.1 Gravimetric Method

Pore volume can be evaluated by the volume of brine saturated in the core. The weight of the dry core and weight of the core after saturated with brine are measured. The pore volume is obtained by dividing the weight difference by brine density.

3.3.1.1.2 Tracer Tests

Purpose

Tracer tests are performed to estimate the pore volume of core sample as well as to examine the homogeneity of the core plug. Tracer tests are conducted before each core flooding test.

Principle

A linear porous medium is initially saturated with synthetic field brine, and then a tracer, which is of similar properties as field brine, is injected into the system at the inlet at a constant rate. In this study, 1% weight of Potassium Nitrate with synthetic field brine is used as a tracer.

This tracer is miscible with field brine and mixing occurs between them. The dispersion dilutes the brine with the tracer and eventually the tracer displaces all the synthetic brine.

If a concentration monitoring device is placed at the downstream outlet, the concentration profile of the tracer would be an S-shaped curve as illustrated in Figure 3-1. If no mixing or dispersion occurs, a piston-like displacement concentration profile would be a step change in concentration. The tracer concentration values are normalized from 0 to 1.

Normalized concentration is calculated as:

$$C_B = \frac{C_B^* - C_{Bo}}{C_{Bi} - C_{Bo}}$$

Where,

C_B = normalized tracer concentration

C_B^* = measured tracer concentration

C_{Bo} = initial concentration of brine

C_{Bi} = maximum tracer concentration

In an ideal longitudinal dispersion model, the concentration profile is symmetric, and at 1.0 pore volume of tracer injection, the concentration is reached at point 0.5.

In order to calculate pore volume, the equal-area technique is used.

First, use the trapezoidal rule to calculate area A1 and A2 under each side of the curve at any point in Figure 3-1.

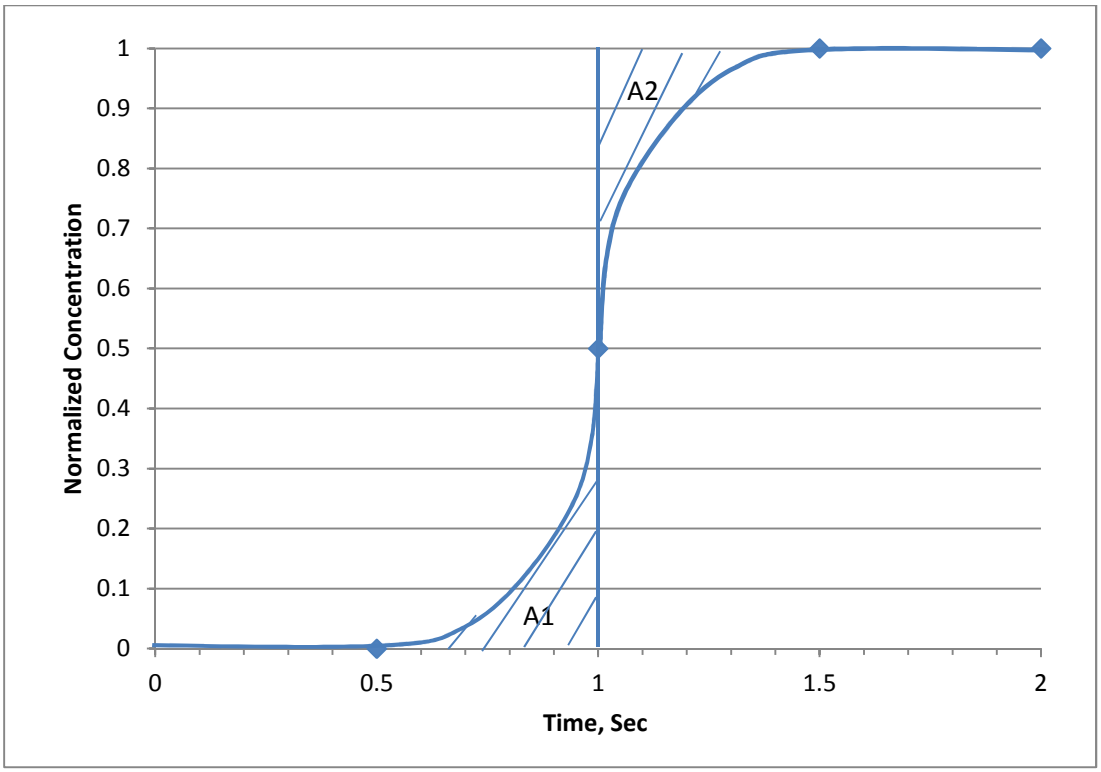

Figure 3-1 Illustration of miscible displacement of brine by tracer and equal area technique

Then, find the time at which A_1=A_2.

Finally, the pore volume (PV) is:

$$PV = \left(t_{eq} - t_o\right) \times q - V_d$$

Where,

V_d = any dead volume (cc)

q = tracer flow rate (cc/min)

t_o = time at which tracer injection starts (min)

t_{eq} = time at which area under each side of the curve is equal, A_1=A_2.

Equipments and Procedures

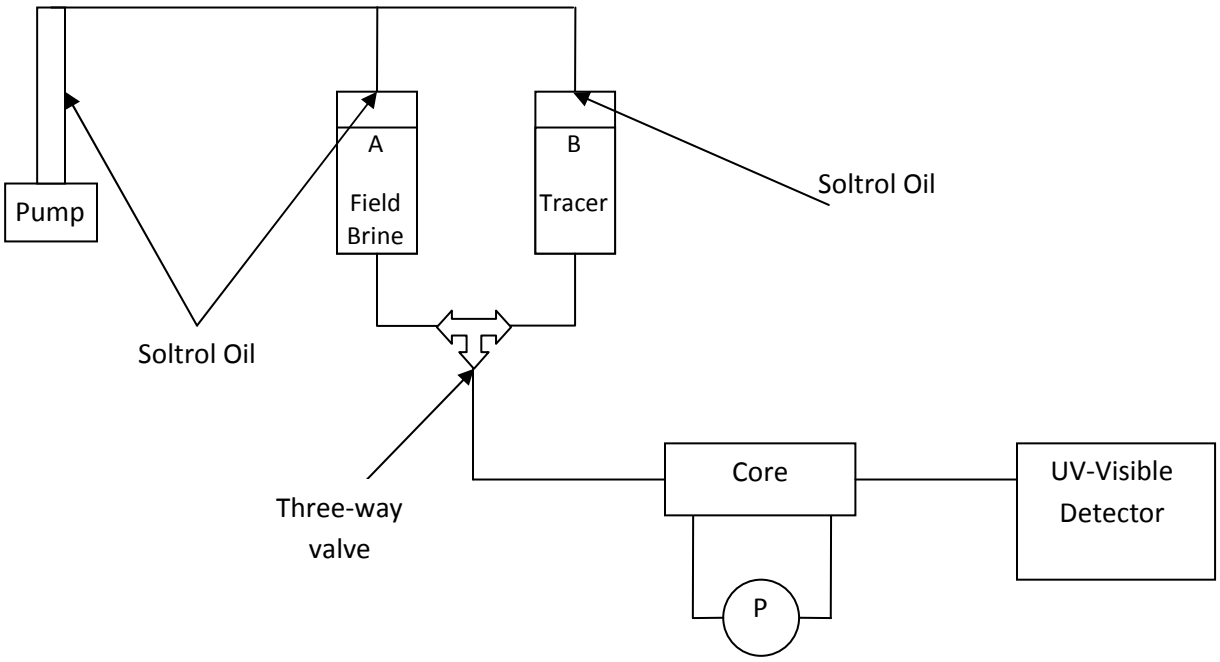

Figure 3-2 Schematic of tracer setup

Figure 3-2 shows the schematic of the tracer test setup. The injection system consists of an ISCO, Inc. 260DM syringe pump and two transfer cylinders. The syringe pump is filled with Soltrol oil. The transfer cylinder A is filled with field brine on bottom and Soltrol oil on top. Transfer cylinder B is filled with tracer on bottom and Soltrol oil on top. The top of transfer cylinder A and B is connected to the syringe pump. The bottom of the two cylinders is connected

to a three-way valve which controls the injection of field brine when it turns to the brine side or the injection of tracer when it switches to the tracer side. The three-way valve is connected to the core inlet. The outlet of the core is connected to an UV-visible detector. A differential pressure transducer is connected to one port at the upstream of the core and the other port at the downstream of the core.

Procedures

At least one hour before the tracer test, the UV-visible detector is turned on and set at a wavelength of 302 nm. Before the tracer test, the flow cell of the detector is cleaned by methylene chloride followed by acetone and then brine injection.

Field brine is injected through the core at a constant flow rate of 1.0 cc/min until the UV-visible detector reads a steady value. Then, the detector is zeroed, the three-way valve is switched to tracer injection and the switch-over time is recorded.

After about 10 PV of tracer injection, the tracer concentration reaches a steady value. Then field brine injection is switched on to displace the tracer solution. The switch-over time is recorded again.

3.3.1.2 Permeability Measurements

Brine is injected through the core at different flow rates for at least 5 PV at each flow rate until the pressure reading across the core is stable, and the pressure drop is recorded. Permeability is calculated according to Darcy's law:

$$k = q\left(\frac{u}{A}\right)\left(\frac{L}{\Delta P}\right)$$

Where,

q = volumetric flow rate of fluid through the core (cc/sec)

k = permeability (Darcy)

A = area (cc)

u = viscosity of the fluid (cp)

ΔP = pressure drop (atm)

L = length (cm)

3.3.2 Core Flooding

Experimental setup

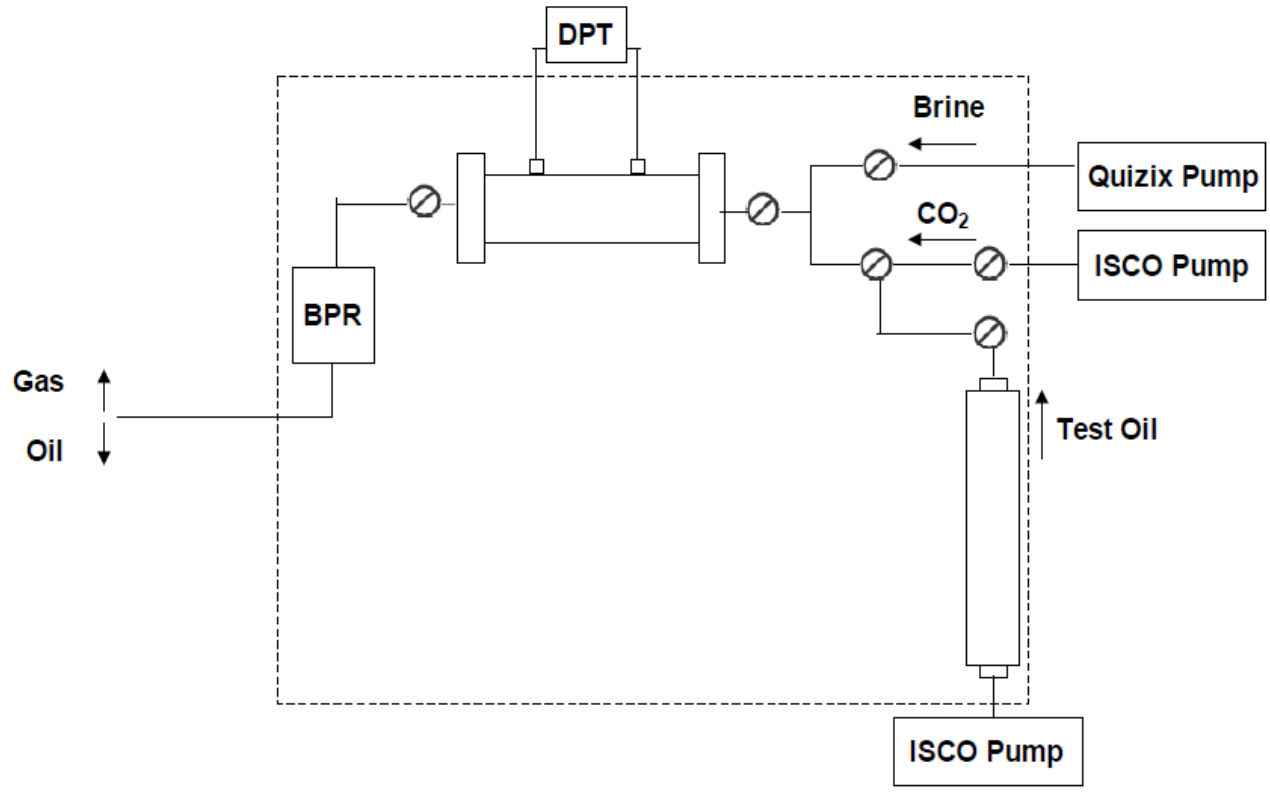

Figure 3-3 Schematic of core flooding setup (Ly Bui, 2010)

Figure 3-3 shows the core flooding setup. It's similar to the slim tube test setup except that a brine injection pump is added, a core holder replaces the slim tube, and one more glassware for outlet fluid collection is added.

The injection system includes two ISCO, Inc. 260DM syringe pumps for CO_2 and crude oil injection at a desired rate, one 485cc transfer cylinder for crude oil storage, and an Eldex pump for synthetic field brine injection.

The system pressure is controlled and maintained by a backpressure regulator (BPR) at the downstream of the core.

The core, oil transfer cylinder, back pressure regulator and other auxiliary equipment are placed inside a Lindbergh/ Blue M oven with a Eurotherm temperature controller. The temperature is set at a constant reservoir temperature of 146°F.

Oil pressure, CO_2 pressure, pressure drop across the core, and back-pressure regulator pressure are measured by four Valydine pressure transducers. The absolute pressure transducers have the capability of measuring pressures up to 2500 psi with the accuracy of 0.25% of their full scale (0-2500 psi) potential while the pressure range of the differential pressure transducer is 50 psi with the accuracy of 0.05% of its full scale potential.

The effluent end of the core is exposed to atmospheric conditions. The separator gas is connected to a flow meter. The fluid is collected by graduated glassware designed for different stages of displacement.

Procedure

Tertiary CO_2 core flooding tests for ETOF reservoir core and Berea sandstone core are performed to investigate the effect of pressure on the oil recovery efficiency. In each set of experiments, core flooding tests are carried out for a range of pressures at the reservoir temperature of 146°F.

The system pressure and temperature, CO_2/oil pressure, pressure drop across the core, gas flow rate, and operating time are recorded by the computer. The initial and final volumes of CO_2 in the pump are recorded manually.

In each run, the core is saturated with field synthetic brine first. Once the system pressure is set at a desired pressure and allowed to equilibrate, the core is saturated with 10 PV of synthetic field brine at 0.5cc/min, 1.0cc/min, 1.0cc/min, and the pressure drop is recorded for different flow rates.

Before oil injection, the field brine flow rate is reduced to 0.5cc/min for equilibration purpose. Then, reservoir oil is injected through the core at 0.5cc/min for at least 10 PV. The volume of brine collected and the pressure drop are recorded.

Water flooding is performed after oil flooding. Brine is injected through the core at 0.5cc/min for at least 10 PV. The volume of oil collected and the pressure drop are recorded.

The CO_2 pump temperature is set by a circulator at the temperature of the system. CO_2 pump pressure is set slightly above the pressure of the back pressure regulator. The CO_2 flow rate is set at a constant rate of 0.1cc/min.

Before CO_2 injection, the brine injection rate is set to 0.1cc/min. Then, CO_2 is injected through the core at 0.1cc/min for at least 10 PV. The volume of oil and water collected and the pressure drop are recorded.

Each set of core flooding tests are conducted from high pressures to low pressures. After each of CO_2 flooding test, the system is depressurized by venting the dome load gas slowly. Then, the system is cleaned by injecting at least 10 PV of methlyene chloride followed by 10 PV of methanol and brine injection, respectively. The entire series of experiment is repeated several times at different pressures but with all other variables held constant. Recoveries are plotted as a function of displacement pressure.

Displacement Rates Selection

A reduction in the CO_2 injection rate was found to improve oil recovery and it was believed that the higher oil recovery efficiency stems from the longer contact time between CO_2 and residual oil and the consequent reduction in oil viscosity and increase in oil swelling (M. Dong et al,

February 2002). In this study, the CO_2 flow rate is selected as 0.1cc/min to achieve good micro scale displacement efficiency in laboratory CO_2 displacement.

3.4 Results and Discussions

3.4.1 Core Characterization Results

Table 3-3 and Table 3-4 show the properties of Berea sandstone core and ETOF reservoir core properties measured before each run of the core flooding tests from high pressures to low pressures. Pore volume was calculated from the tracer test. Reported permeability was calculated based on values averaged from at least three different flow rates when the core is saturated with field brine. In table 3-3, the first two rows are measured in sequent from the same Berea sandstone core. After the second run, 1748psi, the core holder was damaged when preparing for the third run due to core plugging which maybe resulted from severe permeability reduction. The same situation happened in the set of core flooding tests for reservoir core. In table 3-4, the first two rows are measured before the first two core flooding tests for the same reservoir core. After the second run, 1763psi, the core plugging was damaged again and needed to another reservoir core. The third row was measured before the 1386psi test for the second reservoir core.

Berea sandstone core	Pore volume(cc)	Porosity	K(mD)
#Test 1	5.82	0.21	96.91
#Test 2	5.32	0.19	141.98
#Test 3	4.99	0.17	294.17

Table 3-3 Berea core properties

ETOF core sample	Pore volume(cc)	Porosity	K(mD)
#Test 1	5.86	0.17	77.9
#Test 2	4.82	0.14	26.9
#Test 3	6.90	0.22	10.8
#Test 4	5.70	0.17	48.9

Table 3-4 Reservoir core properties

3.4.2 Tracer Tests Results

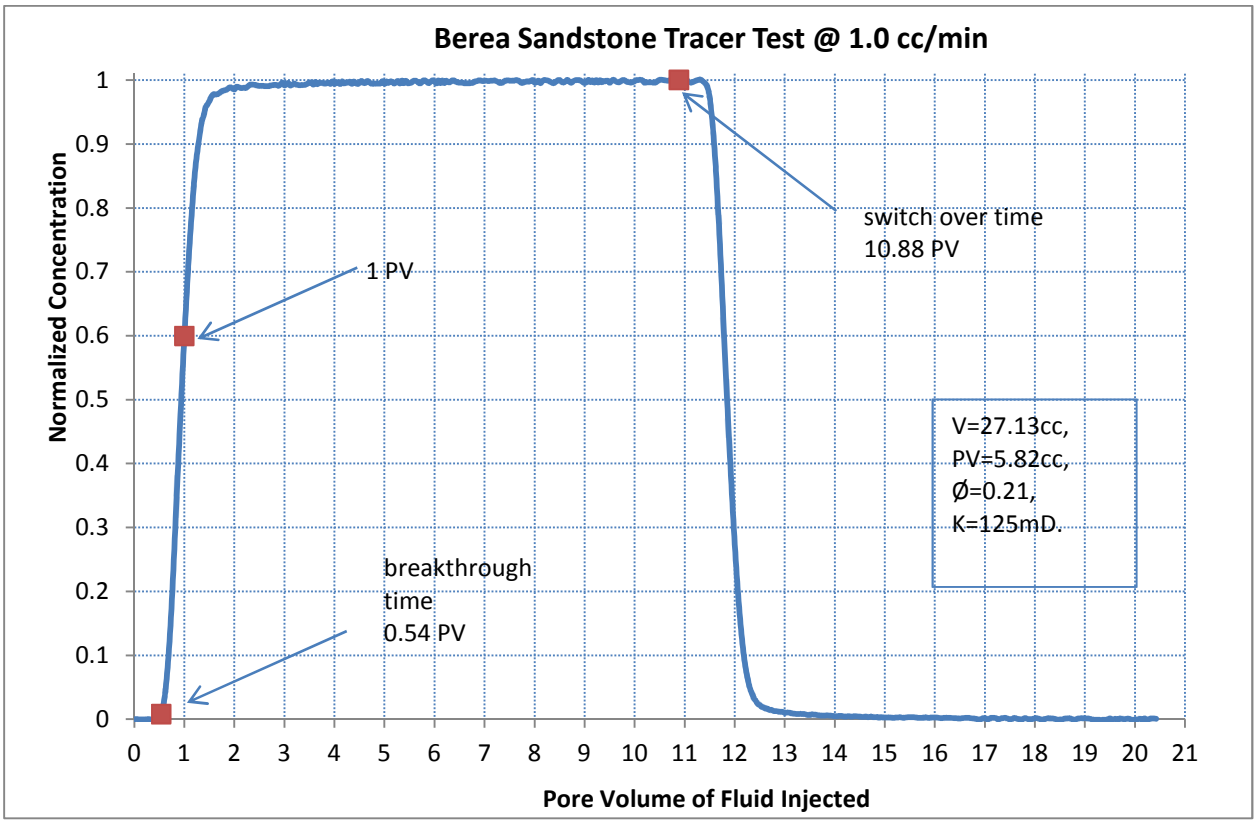

Figure 3-4 Berea sandstone tracer test

Figure 3-4 is a typical Berea sandstone tracer test result. The concentration profile from the Berea core tracer test is relatively symmetric indicating a relatively homogeneous core.

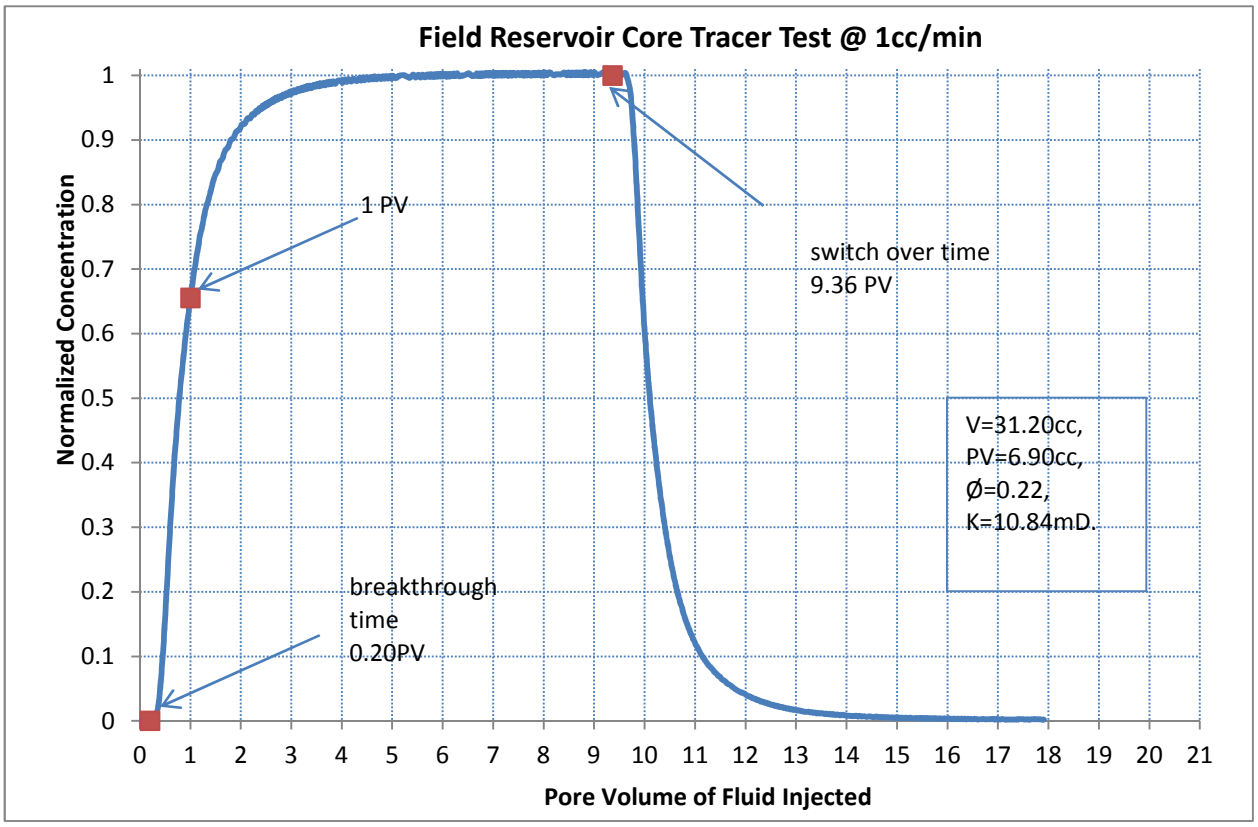

Figure 3-5 ETOF reservoir core tracer test

Figure 3-5 is one of the ETOF reservoir core tracer test plots. Asymmetry of the concentration profile from the reservoir core tracer test is observed. The tracer breaks through early at 0.20 PV compared to 0.54 PV in Berea sandstone core. At 1.0 PV of tracer injection, the concentration reaches to as high as 0.66. Dead-end pore volume, permeability heterogeneities may cause the long dispersion tail and asymmetry of the concentration profile.

3.4.3 Core Flooding Results

Table 3-5 and Table 3-6 summarize CO_2 tertiary core flooding results for Berea sandstone cores and ETOF reservoir cores at 146°F. Calculations of residual water saturation (Swr), residual oil

saturation after water flooding (Sor), and residual oil saturation after CO_2 flooding (Sorc), residual water saturation after CO_2 flooding (Swrc) are based on material balance. Oil recovery of residual oil in place is by volume percentage.

System Pressure	Swr	Sor	Sorc	Swrc	Oil Recovery of ROIP(%)
1945psi	0.16	0.49	0.05	0.49	90.11
1748psi	0.12	0.43	0.07	0.33	83.33
1410 psi	0.28	0.35	0.17	0.41	52.02

Table 3-5 Berea core flooding

System Pressure	Swr	Sor	Sorc	Swrc	Oil Recovery of ROIP(%)
1994psi	0.37	0.50	0.15	0.48	69.97
1763psi	0.22	0.58	0.18	0.40	68.35
1386 psi	0.29	0.58	0.35	0.40	39.70
1122 psi	0.26	0.58	0.44	0.40	24.24

Table 3-6 Reservoir core flooding

Figure 3-6 compares percentage of oil recovery at 10 PV of CO_2 injection changes with pressure for Berea sandstone cores and ETOF reservoir cores.

CO_2 tertiary oil recovery of residual oil in place increases with increasing pressures. The oil recovery efficiencies for Berea sandstone are generally higher than reservoir cores. At MMP, Oil recovery efficiency for Berea sandstone core is 82%, and is 69% for reservoir cores. At current reservoir pressure 1100psi, the oil recovery efficiency for reservoir core is 24% at reservoir temperature of 146°F. CO_2 injection will be immiscible at current reservoir pressure.

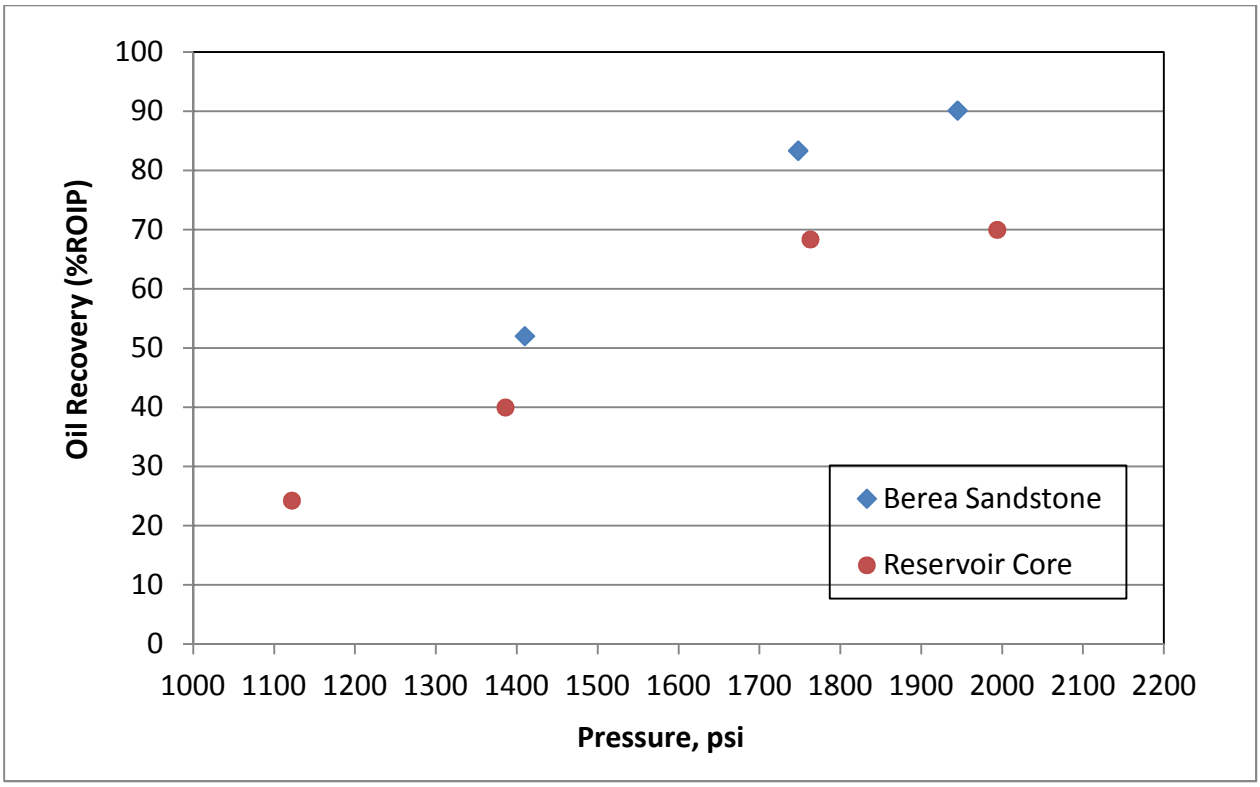

Figure 3-6 Core flooding results

3.4.4 Effects of Asphaltene Deposition

During the CO_2 core flooding in this study, a dramatic permeability decrease and system plugging were observed. It's believed that asphaltene deposition could cause this problem. It's necessary to evaluate asphaltene deposition mechanisms, tendency and amount and study methods to control the deposition.

The asphaltenes are believed to exist in the oil as a colloidal suspension stabilized by resins adsorbed on their surface. As crude oil is produced, this stability may be disrupted by pressure reductions, temperature declines, crude oil chemical composition changes, introduction of

miscible gases and liquids, mixing with diluents and other oils, and during acid stimulation, hot oiling and other oilfield operations. All of the above factors upset the colloidal system and may result in irreversible flocculation of asphaltenes (Y. R. Yin, 2000).

The mixing of crude oil and CO_2 leads to asphaltene deposition and flocculation , and the deposition of asphaltene has been reported to cause severe pore plugging, loss of productivity and injectivity (Y. R. Yin, 2000) (Amirmasoud Kalantari Dahaghi, 2008) (W. A. Limanowka, 2009)(W. A. Limanowka, 1999).

Even in light oils, the asphaltene deposition can be a problem. In fact, the light oils have more potential of asphaltene precipitation than heavy oils even though heavier oils may have a much higher asphaltene content. Because heavier oils dissolve more asphaltene while lighter oils may have lower asphaltene solubility(Amirmasoud Kalantari Dahaghi, 2008) (Shawket Ghedan, 2009).

Besides the asphaltene deposition effects on loss of injectivity and oil recovery, researchers have reported that when asphaltene content in crude oil exceeds a certain point, a significant increase in oil wet conditions takes place (Haung and E.T.S, April 1992) (AI-Maamari et al, April 2000). The mechanism of wettability change due to asphaltene deposition was studied by Martin J. Blunt (Martin J. Blunt, June 2001). According to Blunt, asphaltene is a surface-active component of the oil, which means it will adhere to the surface, exposing the hydrocarbon end and making

the reservoir rock surface oil-wet where oil directly contacts the reservoir rock, while regions with a wetting film of water on the surface remain water-wet.

The asphaltene/resin ratio and high/low molecular weight component ratio determines which crude oil can precipitate asphaltenes because resins keep asphaltene stable in the solution, and asphaltene has a high molecular weight (Shawket Ghedan, 2009).

The onset of asphaltene precipitation and the extent of bulk precipitation can be measured through the Acoustic Resonance Method, the Gravimetric Method and the Light-Scattering Technique (LST) (Shawket Ghedan, 2009). Solid Detection System (SDS) can also detect the onset of asphaltene precipitation, and the bulk deposition can be measured by a filtering system (Fawas M. Al-Otaibi et al, 16-18 April 2012).

Research showed that:

1) The asphaltene flocculation increased linearly in the single phase region with CO_2 concentration after the onset;
2) The higher the permeability of the matrix, the higher the damage of asphaltene precipitation during CO_2 injection;
3) The most damaging place for asphaltene to deposit is in the near wellbore area and inside the ESP pump (Amirmasoud Kalantari Dahaghi, 2008) (Abdulrazag Y. Zekri et al, 2007) (W. A. Limanowka, 1999).

There are many chemicals to treat asphaltene precipitation, such as asphaltene inhibitors, solvents, and dispersants. According to Y. R. Yin (Y. R. Yin, 2000), asphaltene precipitation in a CO_2 flood in West Texas has caused major problems such as tubing plugging, and a new asphaltene precipitation inhibitor was developed to successfully reduce the cost of these damages.

New methods combined with chemical treatments have been developed to control asphaltene deposition. The use of Variable Speed Controllers (VSC) combined with oversized pumps, increased impeller vein heights, internal pump coatings, reduced pressure drop at the pump intake and injection capillary have been successfully applied according to the oil field condition (W. A. Limanowka, 1999).

The severe decreases in core permeability were found after 5 PV of CO_2 injection and after depressurizing the system. This indicated that the mixing of CO_2 with oil and depressurizing the system are two main mechanisms of asphaltene deposition in this study.

Although the onset of asphaltene deposition is not measured in this study, the bulk amount of asphaltene in the crude oil is measured carefully according to ASTM D 893-85 standard procedures:

1. In a sealed sample container, heat crude oil to reservoir temperature and agitate it until the oil is well mixed.
2. Clean, dry and desiccate a 50 ml centrifuge tube. Weigh and record the weight.

3. Accurately weigh approximately 5 grams of crude oil in a centrifuge tube and record the weight.
4. Fill centrifuge tube with heptanes to 50 ml mark.
5. Cap tube and shake it to mix well.
6. Centrifuge the tube for 20 minutes at 1600 rpm.
7. Decant heptanes until the fluid level reaches the 3 ml mark, and add about 10 ml heptanes and agitate the solids with a wire.
8. Fill the tube with heptanes to 25 ml mark, and cap the tube and shake it well.
9. Centrifuge the tube for 20 minutes at 1600rpm.
10. Repeat steps 7 through 9 until decanted liquid is clear in color.
11. Carefully decant the heptanes.
12. Dry the tube and solids in an oven at 105°C for 30 minutes.
13. Cool the tube in desiccators, and measure the weight of the tube with solids in it.
14. Calculate weight percentage of asphaltenes (heptanes insolubles) in the crude oil= grams of dried solids / grams of oil sample *100%

The asphaltene (heptanes insolubles) concentration in crude oil was determined to be 4% by weight. Further assessments need to be done for the onset of asphaltene precipitation in order to control precipitation.

3.4.5 Fluid-Rock Interactions

The permeability and porosity of the cores decreased significantly after each run except the first one, and to the point that the core had to be changed to another one. Other than asphaltene deposition, the fluid-rock interactions may play an important role here and needs to be evaluated. The interactions between CO_2/brine and reservoir rock can have both positive and negative effects.

a) Dissolution of Rock

CO_2 dissolves in water to produce the weak carbonic acid. Then the cementing material such as carbonates in the unconsolidated sandstone rocks would dissolve. As the eluted rock collapses, the dissolved particles in the rock could be plugged in the throat of interstitial pores. Since carbonates are pore-fillings and replacement cements in sandstones, and located between sand grains adjacent to flow channels, a small change in pore framework could result in a significant decrease in permeability (Graham D. Ross et al, 1982). According to Graham Ross (1982), laboratory core flooding experiments under reservoir conditions shows the carbonate dissolution in the rock has a significant impact on the permeability and effluent concentrations. Dissolution severity depends on different textural properties of the rock and acid strength. On the other hand, some researchers found that the dissolution of rock could increase injectivity and permeability if the dissolved particles are smaller than the throat of the pores and be flushed away (Fawas M. Al-Otaibi et al, 16-18 April 2012).

Chemical reactions induced by CO2 injection:

$$CO_2(g) + H_2O = H_2CO_3 \quad \text{-(1)}$$

$$H_2CO_3 = H^+ + HCO_3^- \quad \text{-(2)}$$

The increased acidity induces dissolution of many rock minerals.

b) Accumulation of carbonates in the rock matrix

Accumulation of carbonates in the rock matrix is due to two reasons. First, CO_2 can react with the dissolved minerals from the rock and secondary carbonate mineral precipitates. Also, CO_2 can react with the minerals from the formation brine. This could lead to a decrease in porosity and resulting in a considerable decrease in permeability (Karsten Pruess et al, 2003) (Fawas M. Al-Otaibi et al, April 2012).

Chemical reactions:

$$Ca^{2+} + HCO_3^- = CaCO_3(s) + H^+ \quad \text{-(3)}$$

$$Mg^{2+} + HCO_3^- = CaCO_3(s) + H^+ \quad \text{-(4)}$$

$$Fe^{2+} + HCO_3^- = CaCO_3(s) + H^+ \quad \text{-(5)}$$

Since there are large amounts of Ca2+, Mg2+ cations in the synthetic brine, they would react with CO_2 and form precipitations which contribute to lowering the porosity and inversely lowering the permeability.

Whether the permeability and porosity variation is due to asphaltene deposition, dissolution of rock, secondary carbonate mineral precipitations or the precipitation of some of the brine ions and to what extent do these factors contribute to the decrease is unclear at this point. However, many pinholes and muddy solids were found at the injection face of the reservoir core sample after core flooding and lots of crystals were found at the injection face of the Berea sandstone core sample. The decrease in injectivity is likely due to both dissolution and precipitation.

Abdulrazag Y. Zekri (Abdulrazag Y. Zekri et al, 2007) examined the mineralogical rock composition before and after CO_2 flooding and found a significant reduction in calcium associated with the decrease of permeability which indicates calcium mineral dissolution. He also analyzes the produced water before and after CO_2 flooding and found a drop in calcium ion content indicating the calcium precipitation. He further presents the asphaltene content of initial crude oil and produced oil content to show the amount of asphaltene deposition.

3.5 Conclusions

1. CO_2 reacts with rock in the presence of asphaltene in crude oil and/or water which alters the core permeability.
2. CO_2 tertiary oil recovery of residual oil in place increases with increasing pressures. The oil recovery efficiencies for Berea sandstone are generally higher than reservoir cores. At MMP, Oil recovery efficiency for Berea sandstone core is 82%, and is 69% for reservoir cores.
3. At current reservoir pressure 1100psi, the oil recovery efficiency for reservoir core is 24% at reservoir temperature of 146°F. CO_2 injection will be immiscible at current reservoir pressure. Applying CO_2 EOR in this area is not likely to be profitable.
4. Asphaltene deposition could be a big issue in applying CO_2-EOR.

4. CONCLUSIONS AND RECOMMENDATIONS

4.1 Conclusions

1. From slim tube tests, MMP was estimated to be 1776 psig at 146°F. Miscibility is therefore not achievable at the current reservoir pressure of 1100 psig.
2. At pressures below 1464psi, CO_2 solubility and oil swelling factor increase with increasing pressure as CO_2 dissolves in the oil and the oil expands.
3. Significant extraction starts at 1464 psi. The swelling factor decreases as pressure further increases after this point.
4. Extraction or vaporization of hydrocarbons is the principal mechanism of the multi-contact miscibility development.
5. CO_2 reacts with rock in the presence of asphaltene in crude oil and/or water which alters the core permeability.
6. CO_2 tertiary oil recovery of residual oil in place increases with increasing pressures. The oil recovery efficiencies for Berea sandstone are generally higher than reservoir cores. At MMP, Oil recovery efficiency for Berea sandstone core is 82%, and is 69% for reservoir cores.
7. At current reservoir pressure 1100psi, the oil recovery efficiency for reservoir core is 24% at reservoir temperature of 146°F. CO_2 injection will be immiscible at current reservoir pressure.
8. Asphaltene deposition could be a big issue in applying CO_2-EOR.
9. Unless CO_2 sources are abundant and asphaltene deposition could be controlled by new technology, this reservoir is currently not feasible for CO_2-EOR.

4.2 Suggestions

1. CT scan NMR measurements can be used for core plugs screening in core flooding experiments to make sure there is no fracture or permeability barrier within the plugs and the core plugs are of the same rock type.
2. Mineralogical assessments employing SEM (Abdulrazag Y. Zekri et al, 2007) or other methods can be used to investigate any mineralogical changes due to the interaction between formations brine, CO_2 and reservoir rock.
3. Wettability change can be measured in core flooding tests. Shawket (Shawket Ghedan, 2009) suggests that "with NMR techniques, changes in the T2 relaxation time distribution and calculation of surface reflexivity can often be used for wettability indices. In conventional testing, repeat measurements of the Amott or USBM before and after CO_2 injection provide one point of comparison as do more sophisticated observations based on ESEM images".
4. Analysis of produced water prior and after core flooding can be used to evaluate interactions between CO_2 and brine minerals.
5. Oil analysis before and after CO_2 core flooding can be done during core flooding tests, It not only provides data for simulation comparison and tuning, but also presents quantitatively the amount of asphaltene precipitation. Besides, oil analysis provides data to further understand displacement mechanisms.
6. The onset of asphaltene and amount of deposition can be measured quantitatively to control asphaltene deposition in field operation.
7. The multi-phase fluid flow mechanisms can be further studied using simulation methods.

8. The experimental results could be compared with commercial software such as CMG packages.

REFERENCES

1. U.S oil production potential from accelerated carbon capture and storage, March 2010, Advanced resources international, Inc., Prepared for Natural Resources Defense Council
2. Improving Domestic Energy Security and Lowering CO_2 Emissions with "Next Generation" CO_2-Enhanced Oil Recovery (CO_2-EOR), June 2011, Prepared by Energy Sector Planning and Analysis (ESPA), Vello A. Kuuskraa et al, Advanced Resources International, Inc., DOE/NETL-2011/1504
3. CO_2 as Injection Gas for Enhanced Oil Recovery and Estimation of the Potential on the Norwegian Continental Shelf by Odd Magne Mathiassen, May 2003, NTNU
4. Enhanced Oil Recovery, 1998, Don W. Green and G. Paul Willhite, SPE Textbook Series Vol. 6
5. Laboratory experiments to evaluate field prospects for CO_2 flooding, F.M. Orr Jr., SPE, New Mexico Inst. of Mining and Technology, April 1982, page 892, Journal of Petroleum Technology
6. E. Tzimas et al, DG JRC Institute for Energy Petten, The Netherlands, December 2005, Enhanced Oil Recovery using Carbon Dioxide in the European Energy System
7. F. P Wang, Engineerng and Geologic Characterization of Giant East Texas Oil Field: North and South Pilot Studies, 2008, SPE
8. W. F.Yelling and R. S. Metcalfe, 1980, Determination and Prediction of CO_2 minimum miscibility pressures, SPE
9. Graig A. Williams et al, 1980, Use of the Peng-Robinson Equation of State to Predict Hydrocarbon Phase Behavior and Miscibility for Fluid Displacement, SPE

10. Shawket Ghedan, Global laboratory experience of CO_2-EOR flooding, the Petroleum Institute, 2009, SPE 125581

11. Abiodun Matthew Amao et al, 2012, A New Look at the Minimum Miscibility Pressure (MMP) Determination from Slimtube Measurements, SPE

12. Rahmatabadi, K. A., the roleof interfacial tension in near-miscible CO_2 injection, 2006, p. 107

13. Wei Ren and Aaron M. Scurto, High-pressure phase equilibria with compressed gases, 2007

14. E. W. Lemmon et al, NIST reference fluid thermodynamic and transport properties, REFPROP version 8.0, Gaithersburg, MD, 2007

15. J.S. Tsau, Swellng/extraction test of a small sample size for phase behavior study, SPE, 2010

16. Siagian et al, The extraction of hydrocarbons from crude oil by high pressure of CO_2, SPE, 1998

17. Azita Ahosseini and Aaron M. Scurto, Viscosity of imidazolium-Based Ionic Liquids at Elevated Pressures: Cation and Anion Effects. International Journal of Thermophysics, 2008. 29(4): p. 1222-1243

18. R.B. Bird et al, Transport Phenomena, Wiley, New York, 1960

19. ViscoPro 2000 Viscometer System Operations Manual, Cambridge Viscosity, PAC, www.cambridgeviscosity.com

20. Best practices for conducting CO_2-EOR lab study, Fawas M. Al-Otaibi et al, 16-18 April 2012, SPE 151126

21. Ly Bui, Near Miscible CO_2 Application to Improve Oil Recovery, 2010, University of Kansas

22. M. Dong et al, Coreflood studies of Tertiary CO_2 Flood in Naturally Fractured Midale Formation in Southeast Saskatchewan, February 2002, Volume 41, No. 2, Journal of Canadian Petroleum Technology

23. Y. R. Yin, Asphaltene Inhibitor Evaluation in CO_2 Floods: Laboratory Study and Field Testing, 2000, SPE

24. Formation Damage Through Asphaltene Precipitation Resulting From CO_2 Gas Injection in Iranian Carbonate Reservoirs, 2008, Amirmasoud Kalantari Dahaghi, SPE

25. Asphaltene Deposition Problems in Oil Industry with Focus on Electric Submersible Pump Applications, 2009, W. A. (Andy) Limanowka, SPE

26. W. A. Limanowka, 1999, Asphaltene Deposition Problems in Oil Industry with Focus on Electric Submersible Pump Applications, SPE

27. Haung, E.T.S, The Effect of Oil Composition and Asphaltene Content on CO_2 Displacement, April 1992, SPE

28. Asphaltne Precipitation and Alteration of wetting: Can Wettability change During Oil Production?, AI-Maamari et al, , April 2000, SPE

29. Flow in Porous Media-pore Network Models and Multiphase Flow, Martin J. Blunt, June 2001, Current Opinion in Colloid & Interface Science, 197-207, Elsivier

30. Formation Damage Through Asphaltene Precipitation Resulting From CO_2 Gas Injection in Iranian Carbonate Reservoirs, 2008, Amirmasoud Kalantari Dahaghi, SPE

31. An Experimental Investigation of Interactions Between Supercritical CO_2, Asphaltenic Crude Oil, and Reservoir Brine in Carbonate Cores, Abdulrazag Y. Zekri et al, 2007, SPE

32. Asphaltene Deposition Problems in Oil Industry with Focus on Electric Submersible Pump Applications, W. A. Limanowka, 1999, SPE

33. W. A. Limanowka, 1999, Asphaltene Deposition Problems in Oil Industry with Focus on Electric Submersible Pump Applications, SPE

34. The Dissolution Effects of CO_2-Brine Systems on the Permeability of U.K. and North Sea Calcareous Sandstones, Graham D. Ross et al, 1982, SPE

35. Best practices for conducting CO_2-EOR lab study, Fawas M. Al-Otaibi et al, 16-18 April 2012, SPE 151126

36. Karsten Pruess et al, 2003, Numerical Modeling of Aquifer Disposal of CO_2, SPE

37. An Experimental Investigation of Interactions Between Supercritical CO_2, Asphaltenic Crude Oil, and Reservoir Brine In Carbonate Cores, Abdulrazag Y. Zekri et al, 2007, SPE104750

38. Mechanisms of Miscible Oil Recovery: Effects of Pressure on Miscible and Near-Miscible Displacements of Oil by Carbon Dioxide, J-G. J. Shyeh-Yung, 1991, SPE22651

39. An Experimental Investigation of Interactions between Supercritical CO_2, Asphaltenic Crude Oil, and Reservoir Brine in Carbonate Cores, Abdulrazag Y. Zekri et al, 2007, SPE104750